Galvanic microencapsulation: A new technique to suppress pyrite oxidation

A dissertation submitted in partial fulfillment of the requirement for the degree of Doctorate in Engineering

Sophea Seng

Division of Sustainable Resources Engineering,
Graduate School of Engineering,
Hokkaido University, Japan

March 2019

ABSTRACT

Acid mine drainage (AMD) is one of the biggest environmental concerns for centuries. This problem is generally caused by the exposure of sulfide minerals to oxygen and water. This process can occur naturally, however, mining industries are the major producer of such effluents. AMD is very acidic and contains high concentrations of hazardous heavy metals such as copper (Cu), lead (Pb), and zinc (Zn) as well as toxic metalloids like arsenic (As) and selenium (Se). The most widely used technique to mitigate the negative environmental impacts of AMD is via neutralization. In this technique, basic materials such as limestone are added to AMD to increase its pH and precipitate most of the heavy metal as metallic oxyhydroxides. Even though this technique is effective, AMD generation could continue for several decades or even centuries, so this approach is unsustainable. Microencapsulation is a promising and potentially more sustainable approach because it limits AMD production by suppressing pyrite oxidation directly through the formation of a passivating coating on the mineral. This study developed a new technique to prevent pyrite oxidation called "Galvanic Microencapsulation".

Chapter 1 gives a general introduction of acid mine drainage (AMD) formation and its mechanism as well as reviews AMD remediation, and prevention techniques. The statement of the problem and the objective of the study are highlighted to understand the key points and the structure of the entire research. The prevention techniques to prevent AMD are formation by controlling the migration of water, flooding and sealing of underground mine, alkaline amendment, alkaline recharge trenches, anaerobic and anaerobic wetland, limestone ponds, in-pit disposal, and encapsulation. Among these techniques microencapsulation to prevent pyrite from being oxidized by forming a protective coating on pyrite surface is recently gaining attention. The original microencapsulation techniques introduced by Evangelou (1995) used hydrogen peroxide (H_2O_2) to oxidize Fe^{2+} to Fe^{3+} for the formation of insoluble ferric phosphate on pyrite. Although this technique effectively suppressed pyrite oxidation, H_2O_2 was unable to selectively target pyrite in real, complex wastes leading to unnecessarily large consumption of expensive reagents. Moreover, handling and storage of H_2O_2 are both difficult, especially in large-scale applications. Carrier microencapsulation (CME) is, a microencapsulation technique that uses redox-sensitive metal(loid)-organic complexes to carry the coating material to the surface of pyrite where the complexes are adsorbed and decomposed, releasing the insoluble metal(loid) ion of the complex that is rapidly precipitated to form a protective coating on pyrite. Because pyrite dissolves via an electrochemical mechanism, the redox-sensitive metal (loid)-organic complexes have been shown to selectively target pyrite even in a complex system containing arsenopyrite and quartz.

Chapter 2 introduces a new encapsulation technique called galvanic microencapsulation (GME). The effects of GME on pyrite oxidation using zero-valent aluminum (ZVAl) or zero-valent iron (ZVI) at various dosages and under different conditions (i.e., leaching time and pH) were investigated. Pyrite oxidation was suppressed in the presence of ZVAl or ZVI. Galvanic interaction between pyrite and ZVAl in the first 3 days was negligible, which could be attributed to the Al-oxyhydroxide coating on ZVAl. After 7 days, however, ZVAl exhibited substantial suppressive effects on pyrite oxidation. In comparison, the suppressive effects of ZVI on pyrite oxidation were observed after just 1 day. Pyrite oxidation suppression mechanisms by GME during leaching were elucidated by electrochemical measurements. Cyclic voltammetry and chronoamperometry measurements showed that the suppressive effects of ZVAl and ZVI were predominantly due to galvanic interactions.

In chapter 3, coating formation technique for prolonged suppressive effects of GME on pyrite oxidation using phosphate and ZVI was developed. In Chapter 2 galvanic interaction was observed, however, the coating was not observed on the pyrite surface. In the presence of phosphate, suppression of pyrite oxidation by ZVI was dramatically improved because of the combined effects of galvanic interactions and coating formation. When phosphate was added, ferric phosphate was formed as a protective coating on pyrite.

In chapter 4, GME was applied not only to improve the separation efficiency during coal cleaning but also to suppress pyrite oxidation. GME treatment was carried out before flotation to change the surface of pyrite from hydrophobic to hydrophilic by phosphate coating. Iron phosphate coating was induced in a ball mill grinding system using steel balls as the electron donor and then followed by flotation. The results showed improvement of flotation results and suppression of pyrite oxidation.

Finally, chapter 5 gives the general conclusions of this study.

CONTENTS

LIST OF FIGURES

LIST OF TABLES

CHAPTER 1: GENERAL INTRODUCTION

1.1 Problem statement and objectives

Acid mine drainage (AMD) or acid rock drainage (ARD) is one of the biggest environmental concerns of the mining industry in recent years. For example, it was reported in 1993 that more than 12,000 km of streams were affected by coal mines in northeastern USA United (State Environmental Protection Agency, 1997). Pennsylvania and West Virginia were the states greatly affected and the cost of reclamation was estimated at 1.5 billion US dollars in Pennsylvania alone (Rossman et al., 1997). The major cause of AMD is the exposure of sulfide minerals to oxygen and water. Acid mine drainage can occur naturally, however, mining activities exacerbate this problem because of the exposure of sulfide minerals from their wastes. AMD is very acidic, contains high concentrations of heavy metals such as cobalt, lead, nickel, iron, and manganese as well as toxic metalloids like arsenic (Akcil et al., 2006, Riley et al., 2009, Rossman et al., 1997). Within the sulfide-mineral group, pyrite is the most common gangue mineral found in sulfide mines.

The most commonly used AMD treatment method is neutralization, a process whereby basic substance like limestone or quicklime are mixed with AMD to raise its pH and precipitate most of the metals. Although effective, this approach is unsustainable because it requires continuous and long-term treatment. Sasaki and Igarashi (2013), for example, estimated the length of time necessary for reducing the zinc (Zn) concentration below environmental standard in the AMD of a 40-year old tailings dam by geochemical modeling. They found that it would take more than 1,000 years for Zn to drop below 5 mg/L using very conservative assumptions in their model. In other words, a more sustainable technique is needed to mitigate the AMD problem.

In this study, galvanic microencapsulation (GME) using zero-valent iron (ZVI) and zero-valent aluminum (ZVAl) is proposed as a new technique to limit the formation of AMD by suppressing pyrite oxidation, which is the main cause of AMD formation. There are two important steps in GME: (1) galvanic interaction, and (2) coating formation.

In this chapter, conventional water treatment methods to manage AMD as well as prevention techniques like microencapsulation are reviewed, the concept of GME is introduced and the contents of this thesis are outlined.

1.2 Literature review of acid mine drainage formation and its remediation or prevention

1.2.1 Acid mine drainage (AMD) and its formation

Acid mine drainage (AMD) is one of the biggest environmental concerns for centuries. The cause of AMD is the exposure of sulfide minerals to oxygen and water. AMD is very harmful to the environment because it is very acidic and contains high concentrations of heavy metals and other toxic elements, which could contaminate surface, groundwater and soil (Akcil et al., 2006, Evangelou, 2001, Peppas et al., 2000).

The sources of AMD in mine sites include the mine waste rock dumps, mine tailings, heap leach pads, mine adits, open-cuts, and pit walls. In the case of waste rock and tailings, AMD may come from spoil piles, ore stockpiles, and spent heap-leach piles (MEND, 1996).

To clarify AMD formation, many researchers have been investigating the mechanisms of pyrite oxidation. Eq. 1.1 is the oxidation of pyrite by oxygen and water, a process that releases ferrous ion (Fe^{2+}), sulfate (SO_4^{2-}) and protons (H^+). In the environment where O_2 is abundant or in the presence of iron-oxidizing bacteria, Fe^{2+} is rapidly oxidized to ferric ion (Fe^{3+}) (Eq. 1.2). Other factors that affect the rate of acid generation (Eq. 1.1 and 1.2) include the temperature, solution pH (Smith and Shumate, 1970), the surface area of pyrite (Singer and Stumm, 1968) and the presence of other oxidants such as Mn^{3+} or Mn^{4+}. At pH greater than 4, the oxidation rate of Fe^{2+} to Fe^{3+} is very rapid and but the latter is quickly precipitated as iron hydroxide ($Fe(OH)_3$) (Eq. 1.3) (Stumm and Morgan, 1981). At pH lower than 3.5, the oxidation rate of Fe^{2+} to Fe^{3+} is very slow, so both of these dissolved Fe species exist in solution. The Fe^{3+} from Eq. 1.2 is also known to oxidize pyrite according to Eq. 1.4.

$$FeS_2 + 3.5\ O_2 + H_2O = Fe^{2+} + 2\ SO_4^{2-} + 2\ H^+ \quad (1.1)$$

$$Fe^{2+} + 0.25\ O_2 + H^+ = Fe^{3+} + 0.5\ H_2O \quad (1.2)$$

$$Fe^{3+} + 3\ H_2O = Fe(OH)_3 + 3\ H^+ \quad (1.3)$$

$$FeS_2 + 14\ Fe^{3+} + 8\ H_2O = 15\ Fe^{2+} + 2\ SO_4^{2-} + 16\ H^+ \quad (1.4)$$

1.2.2 Remediation/prevention of acid mine drainage

The AMD treatment methods could vary from one mine to another mine, this variation depends on the location and the availability of the treatment materials. Prevention strategies for AMD include the control of water migration, separation, and blending of wastes with other alkaline

materials, and the use of dry or water covers (Filipek et al., 1996, MEND, 1993, MEND, 1996, USEPA, 1995).

Table 1.1 AMD prevention methods

Target	**Prevention strategy**
Water flow	Diversion ditches, gout curtains, slurry walls
Reduction of water inflow	Encapsulation, capping and sealing. E.g., Dry (soil) covers, liners or coating or permafrost.
Exclusion of oxygen	Water covers (flooding) and sub-aqueous deposition.
	Encapsulation, capping and sealing or permafrost
pH control	Waste segregation and blending
	Alkaline additives
Sulfide removal and isolation	Conditioning of tailings and waste rock
Control of bacterial action (anionic surfactants)	Bactericide
Water treatment	Alkaline amendment
Microencapsulation	Coating of sulfide minerals with protective layers

1.2.2.1 Control of water flow

Water flow control is a strategy whereby clean water (ground and surface water) is prevented from moving through potential acid generating wastes that release metals and acidity (Watson, 1996). In theory, methods such as grout curtain, slurry walls, and diversion ditches could prevent groundwater flow. Generally, large storage dams are built to collect water from waste dumps and ore stockpiles at the site. In the case of contaminated runoff water, it will be treated using an appropriate method such as lime addition. This treated water can be reused or stored in the water storage dam or discharged to the environment.

1.2.2.2 Flooding and sealing of underground mine

(i) Dry covers, soil covers, and liners

Cover, caps, and seal used to limit or eliminate the infiltration of oxygen and water and to isolate sulfide-bearing wastes. Dry soil covers, constructed using either single or multiple layers, are effective when the materials used have very low hydraulic conductivity and high moisture retaining properties (MEND, 1995, Yanful and Nicholson, 1991). A single layer soil cover is often used in low rainfall areas, which can be effective to prevent water from percolating into the waste dump while the multilayered soil approach is useful in high rainfall areas (>50 cm). The ideal dry cover is consists of the following layers: (1) revegetated soil layer to retain moisture, maximize evapotranspiration of water, decrease infiltration and improve resistance to erosion, (2) a second layer composed of course materials to provide lateral drainage of infiltration, (3) a third layer of compacted clay to prevent oxygen penetration, and (4) compacted alkaline layer used to neutralize any acidic leachates formed (Fig. 1.1).

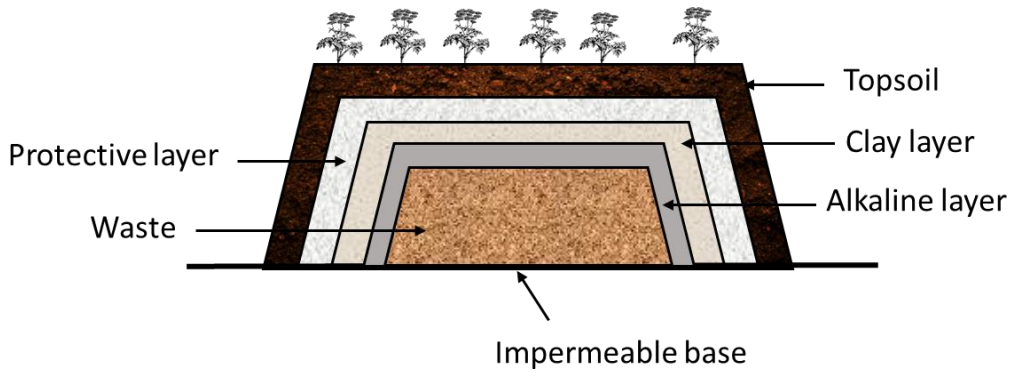

Fig. 1.1 Layout of a dry cover.

(ii) Water cover

Water cover is another alternative to dry cover because the solubility of oxygen and diffusion rate of oxygen is very slow in water, so the oxidation of reactive waste can be minimized. However, the application of this technique is dependent on the site condition such as hydrology, topography and the availability of water sources suitable for water cover application (Dave, 1992, St-Germain and Kuyucak, 1998). The most common application of this method is to deposit the waste in manmade engineered pond to flood the existing tailings pond by designing and constructing appropriate dykes and dams. Even though it could reduce acid generation, a slow release of metals still occurs and over time, the metal concentration will increase and exceed water standards (Aube et al., 1995). The water cover can be improved by using an organic layer, which is called

biological supported water cover. This organic layer could act as a barrier to oxygen and metal release. The organic materials consumed oxygen through bacterial activity and precipitation of metal sulfide phases through anaerobic sulfate-reducing bacteria (Beckett, 1998, St-Germain and Kuyucak, 1997). The Ontario Rio Algom mine uses a water cover of over 65-ha with a water depth of 0.5 to 1 m (Dave and Vivyurka, 1994). Over 50% of the sulfidic uranium tailings are treated with limestone. Lime slurry was added into the inflow water to the flooding cell for additional neutralization. The surface water pH of the flooded cell is 7 with an average acidity of 7 mg/L.

(iii) Separation and blending

The separation method is to separate acid-generating waste from oxidants and blending method is to blend acid-generating waste with alkaline materials.

One of the separation methods is the desulfurization of tailings. This technique requires simple flotation to remove sulfide minerals and disposed of in proper storage. This technique is more effective for pyrrhotite wastes rather than those containing pyrite (MEND, 1996).

Sulfur-oxidizing bacterial also play an important role in AMD generation. Methods such as anionic surfactants are used to control the catalytic effect of bacteria of the oxidation of Fe^{2+} to Fe^{3+}. The bactericides can be applied to refuse conveyor belts or sprayed by trucks on a cell of acid producing wastes. This technique was used in Pennsylvania in 1988. The data showed that 79% reduction of acidity and 82% decrease in dissolved Fe was achieved (Parisi et al., 1994).

1.2.2.3 Alkaline amendment

The alkaline amendment is a modification of the concept to blend acid-producing and acid-neutralizing rocks. Several versions of this technique have been successfully used to treat AMD at the mine site.

Anoxic limestone drain (ALD) is built by using limestone gravel as a bed (low maintenance once it built) and allow AMD to flow through the bed (Fig. 1.2). Limestone is relatively cheap and a readily available source of alkalinity. The ALD process was applied in Paint, Pennsylvania in 1990, which increased the AMD pH from 4.7 to 6.2, alkalinity from 25 to 255 mg/L ($CaCO_3$) while decreasing the Fe total from 208 to 168 mg/L and Al from 0.6 to 0.2 mg/L.

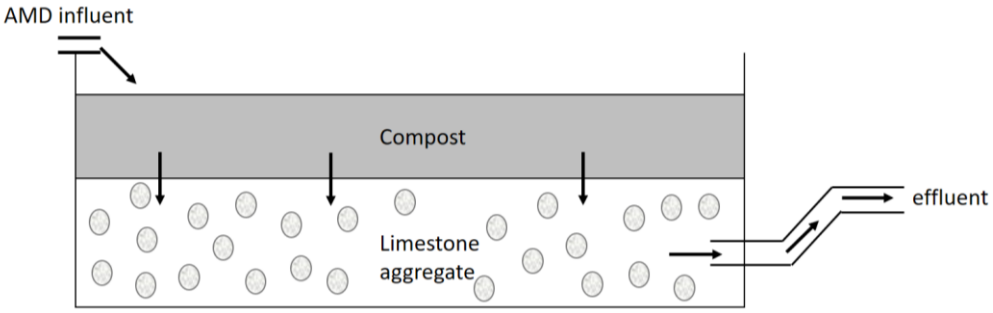

Fig. 1.2 Schematic layout of a reducing and alkalinity producing system (RAPS). (Younger et al., 2003)/

Permeable reactive barriers (PRBs) are used to treat a wide range of polluted groundwater. This process involved with digging a trench or pit along the path of contaminated groundwater and filling it with reactive materials (organic solid and limestone). The reductive microbiological processes in the PRB generated alkaline and remove metals as sulfides, hydroxides, and carbonates (Fig. 1.3). In Northumberland, England PRB was used to treat acidic waste from coal mine (Shilbottle Colliery). The PRB consist of 25% compost horse manure and straw, 25% green waste compost, and 50% limestone gravel. In recent years, more effective PRB was developed using zero-valent iron (ZVI) to treat wastewater and groundwater. PRB using ZVI successfully degraded large number of COCs (TEC, trichloroethylene, tetrachloroethylene, vinyl chloride, carbon tetrachloride and polychlorinated biphenyls), NACs (NB. TNT, 2,4-dinitrotoluene, and 2,6-dinitrotoluene), arsenic, heavy metals (Cr(VI), Ni^{2+}, Pb^{2+}, Cu^{2+}, and Zn^{2+}), and nitrate (Bitrtna et al., 2010, Calabrò et al., 2012, Cho et al., 2010, Choi et al., 2012, Gu et al., 2010, Hwang et al., 2011, Kishimoto et al., 2011, Mitra et al., 2011, Neumann et al., 2013, Sam et al., 2013, Shi et al., 2011, Suzuki et al., 2012, Tseng et al., 2011, Wei et al., 2012, Xiao et al., 2011, Yin et al., 2012).

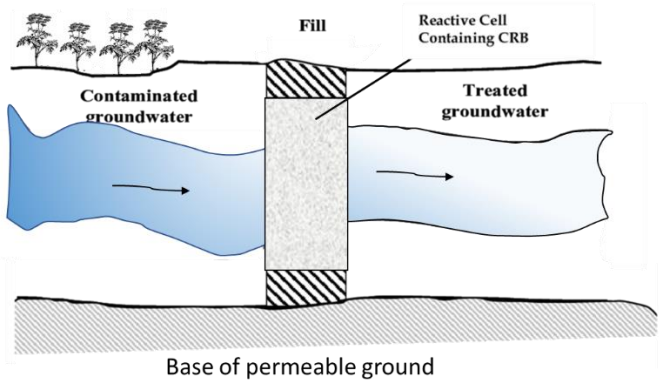

Fig. 1.3 Schematic cross-section of permeable reactive barrier (PBR). (Younger, 2000)

1.2.2.4 Alkaline recharge trenches

The alkaline surface trench is used to minimize or eliminate acid seeps by constructing surface ditches filled with alkaline materials (Caruccio et al., 1984). Nawrot (1994) reported that this method was used to cover 8-ha of coal refuse deposit waste. After installing alkaline surface trench, AMD seeping into the surface water was reduced from 25 to 99% and the Fe concentration decreased from 70 to 90%.

1.2.2.5 Aerobic and anaerobic wetlands

Many researchers showed that biological and chemical process occurring in the wetland can improve the chemical composition of AMD. These constructed wetlands for water treatment are low maintenance and low cost (Kleinmann et al., 1983). Stark (1996) reported that constructed wetland successfully removed metals such as Fe, Mn and Al. The mechanism of reaction in the wetland are (1) formation of metal oxide and oxyhydroxide, (2) formation of metal sulfide, (3) organic complexation reaction, (4) exchange with the other cations on negatively charged minerals/phases, and (5) direct uptake by plants.

Aerobic wetlands are shallow systems that operate by surface flow. Macrophytes are planted in the treatment cells to regulate water flow and to stabilize the accumulation of ferric precipitates. The reactions of the system are:

$$4\ Fe^{2+} + O_2 + 4\ H^+ = 4\ Fe^{3+} + 2\ H_2O \qquad (1.5)$$

$$4\ Fe^{3+} + 12\ H_2O = 4\ Fe(OH)_3 + 12\ H^+ \qquad (1.6)$$

This system also removes arsenic (As) from arsenopyrite (FeAsS) present in mine water. In mine water arsenic present as As^{5+} which mostly adsorbed by the positively charge ferric oxyhydroxides. Tennessee Valley Authority (TVA) have reported the treatment of AMD generated by mine spoil, coal slurries, and coal ash (Brodie et al., 1993) by divided into several stages such as ALD, followed by two or three aerobic wetland cells, and another two or three aerobic wetland cells. A series of this treatment decreased the Fe concentration from 70 mg/L to <0.7 mg/L but was ineffective in Mn removal (Stark et al., 1994).

The anaerobic wetlands/compost bioreactors are opposite to aerobic wetlands and are enclosed below the ground level by compost and do not support any macrophytes. The organic matrix itself supply electron for the reductive reactions. The organic materials could be varying depending on local availability, generally, the composts prepared by mixing biodegradable materials (cow or horse manure) with recalcitrant materials (sawdust, peat, or straw). The variant on the basic compost bioreactor is the reducing and alkalinity producing system (RAPS). The mechanism and efficiency of AMD treatment varies seasonally and with wetland age. Microbial mechanism and alkalinity become critical over long-term AMD treatment if the wetland receives high acid (>300 mg/L), therefore it is more successful to treat small AMD flow.

1.2.2.6 Encapsulation

Microencapsulation is a promising and potentially more sustainable approach because it limits AMD production by suppressing pyrite oxidation directly through the formation of a passivating coating on the mineral. The first encapsulation technique was developed by Evangelou (2001) by forming ferric phosphate coating on pyrite surface using hydrogen peroxide (H_2O_2) to oxidize Fe^{2+} to Fe^{3+}.

Another microencapsulation technique is using lipid that has hydrophobic tails to suppress pyrite oxidation in acidic condition by Alicia et al. (2003). The head group of the lipid is hydrophilic when interacting with water and a hydrophobic tail (Cheng et al., 1998, Sackmann, 1996). Pyrite oxidation suppresses due to the lipid impeding during the pyrite oxidation process.

Carrier microencapsulation (CME), a microencapsulation technique developed by Satur et al. (2007), uses redox-sensitive metal(loid)-organic complexes to carry the coating material to the surface of pyrite where the complexes are adsorbed and decomposed, releasing the insoluble metal(loid) ion of the complex that is rapidly precipitated to form a protective coating on pyrite. Because pyrite dissolves via an electrochemical mechanism, the redox-sensitive metal(loid)-organic complexes have been shown to selectively target pyrite even in a complex system containing arsenopyrite, pyrite, and quartz (Park et al., 2018a, b).

1.3 Concept of Galvanic Microencapsulation (GME)

Although many techniques have been developed and used to treat AMD, most of them are unsustainable because they require continuous and long-term treatment. Sasaki and Igarashi (2013), for example, estimated the length of time necessary for reducing the Zn concentration

below environmental standard in the AMD of a 40-year old tailings dam by geochemical modeling. They found that it would take more than 1,000 years for Zn to drop below 5 mg/L using very conservative assumptions in their model. In other words, a more sustainable technique is needed to mitigate the AMD problem. A better technique for preventing AMD is encapsulation. However, Evangelou and coworkers (1996) used hydrogen peroxide (H_2O_2) which is difficult to apply in the plant because H_2O_2 could not target pyrite and very difficult to handle. One current limitation of the CME technique is the use of catechol, which when oxidized in the presence of DO and metal ions like Fe^{3+} and Cu^{2+}, forms semiquinone radicals, superoxides, and H_2O_2 that are toxic to cells (Schweigert et al., 2001).

In this study, galvanic microencapsulation (GME) using zero-valent iron (ZVI) and zero-valent aluminum (ZVAl) is proposed as a new technique to limit the formation of AMD by suppressing pyrite oxidation, which is the main cause of AMD generation. There are two important steps in GME: (1) galvanic interaction, and (2) coating formation. Galvanic interaction occurs when pyrite interacts with metals or other sulfide minerals having lower rest potentials. In this process, metals or minerals with lower rest potential become the anode and dissolve while the one with higher rest potential becomes the cathode and is protected from dissolution (Fig. 1.4). In GME, ZVI and ZVAl have lower redox potential than pyrite, so they could prevent oxidation of pyrite by dissolving instead of this mineral. As illustrated in Fig. 1.4a, the metal that has lower rest potential than pyrite act as an anode and supply electron for pyrite and is galvanically protected. Fig 1.4b shows that when ZVI or ZVAl is oxidized, the released ions could form metal oxyhydroxide coating on pyrite under certain conditions, which protects the mineral from further oxidation.

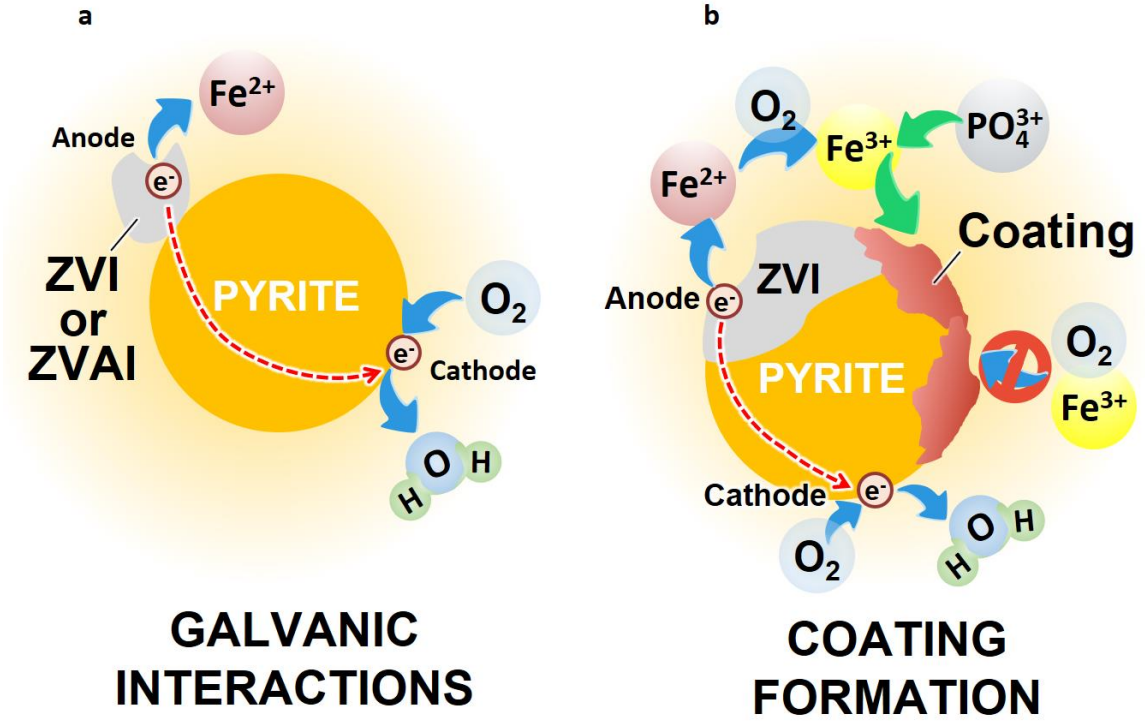

Fig. 1.4 Schematic diagram of (a) galvanic interaction, and (b) coating formation.

1.4 Objectives of this study

i. To introduce a new encapsulation technique called galvanic microencapsulation (GME) using zero-valent aluminum (ZVAl) or zero-valent iron (ZVI),

ii. To investigate the effects of ZVAl and ZVI on pyrite oxidation,

iii. To improve a coating formation on pyrite using ZVI and phosphate,

iv. To apply GME treatment in a ball mill system to improve the separation efficiency during flotation (e.g., coal cleaning).

REFERENCES

Ata. A. and Soner, K.. (2006), Acid mine drainage (AMD): causes, treatment and case studies, Journal of Cleaner Production. (1139-1145).

Aube, B.C., St-Arnaud, L.C., Payant, S.C., YanfulE, K. (1995). Laboratory evaluation of the effectiveness of water covers for preventing acid generation from pyrite rock. In: Proceedings of Sudbury. Minign and the environment, May 1995, Sudbury, Ontario, Canada, Vol. 2 (495-504).

Becckett, P. (1998). Mineral processing and extractive metallurgy review, Eds: F.M. Doyle and N Arbiter Montana, USA, (39-46).

Bhattacharya, J., Islam, M., Cheong, Y. W. (2006). Microbial growth and action: implications for passive bioremediation of acid mine drainage. Mine Water and the Environment. 25 (233-240).

Biterna, M., Antonoglou, L., Lazou, E., Coutsa, D. (2010). Arsenic removal from waters by zero-valent iron: batch and column tests, Chemosphere. 78 (7-12).

British Columbia Task Force. (1989). Draft acid rock drainage technical guide, Ed: Steffen, Bobertson, and Kristen Inc., Vancouver, British Columbia, Canada, August 1989.

Brodie, G.A., Britt, C.R., Tomaszewski, T.M., Taylor, H.N. (1993). Anoxic limestone drains to enhance performance of aerobic acid drainage treatment wetland: experience of the Tennessee valley authority. p. 129-145. In: G.A. Moshiri, (ed.), Constructed Wetland for Water Quality Improvement. Lewis Publisher, Boca Raton, FL. (632).

Calabrò, P.S. Moraci, N., Suraci, P. (2012). Estimate of the optimum weight ratio in zero valent iron/ pumice granular mixture used in permeable reactive barriers for the remediation of nickel contaminated groundwater. J. Hazard. Mater. 207-208 (111-116).

Caruccio, F.T., Geidel, G., Williams, R. (1984). Induced alkaline recharge zones to mitigate acid seeps. P 43-47. In: Processing, national symposium on surface mining, Hydrology, sedimentology and reclamation, 7-10 Dec. 1984, Univ. of Kentucky, Lexington, KY.

Cho, Y. and Choi, S.I. (2010). Degradation of PCE, TCE, and 1,1,1-TCA by nanosized FEPd bimetallic particles under various experiment conditions, chemosphere. 81 (940-945).

Choi, K. and Lee, W. (2012). Enhanced degradation of trichloroethylene in nano-scale zero-valent iron Feton system with Cu (II). J. Hazard. Mater. 211-212 (146-153).

Dave, N.K. (1992). Water cover on acid generating mine/mill wastes: A technical review, CANMET Report, MSL 89-107, Ottawa, Ontario, Canada.

Evangelou, V.P. (2001), Pyrite microencapsulation technology: Principles and potential field application, Ecological Engineering. (165-178).

Donald, S.B., Holl, N., Landine, P., Welch, D. (1997). Recent hydrogeological development in uranium mine tailing management in Canada: the key lake experience, in IAEG international symposium on Engineering geology and the environment, Athens, Greece, June. (23-27).

Filipek. (1996). Acid rock drainage control, J of Mining Environmental Management.

Hwang, Y.H., Kim, D.G., Shin, H.S. (2011). Mechanism study of nitrate reduction by nano zero valent iron, J. Hazard. Mater. 185 (1513-1521).

Kishimoto, N., Iwano, S., Narazaki, Y. (2011). Mechanistic consideration of zinc ion removal by zero-valent iron, Water Air Soil Pollut. 221 (183-189).

Kleinmann, R.L.P., Tiernman, T., Selch, J.G., Harris, R.L. (1983). A low coat low maintenance treatment system for acid mine drainage using Sphagnum moss and limestone. P. 241-245. In:1983 symposium on surface mining, hydrology, sedimentology, and reclamation, 5-9 Dec. Univ. of Kentucky, Lexington, KY.

MEND, (1996). Summary notes MEND workshop. Dry covers technology for acid mine drainag, Sudbury, Ontario, April 15-16 (1996).

MEND, (1995). Literature review report: possible means of evaluating the biological effects of sub-aqueous disposal of mine tailing. (2.11.2a).

MEND, (1995). Reclamation of sulfide tailing using municipal solid waste compost. (2.25.1b).

Meek, F.A. (1994). Evaluation of acid prevention technique used in surface mining. P 41-48. In: Internation land reclamation and mine drainage conference, 24-29 April 1994, USDI, Bureau of Mines SP 06B-94, Pittsburgh.

Mitra, P., Sarkar, D., Chakrabarti, S., Dutta, B.K. (2011). Reduction of hexa-valent chromium with zero-valent iron: batch kinetic studies and rate model, chem. Eng. J.171 (54-60).

Moses, C.O., Nordstrom, D.K., Herman, J.S., Mills, A., (1987). A aqueous pyrite oxidation by dissolved oxygen and by ferric iron. Geochim. Cosmochim. Acta 54 (471-402).

Neumann, A., Kaegi, R., Voegelin, A., Hussam, A., Munir, A.K.M., Hug, S.J. (2013). Arsenic removal with composite iron matrix filters in Bangladesh: a field and laboratory study, Environ. Sci. Technol. 45 (4544-4263).

Nicholson, R.V., Gillham, R.W., Reardon, E.J., (1989a). Pyrite oxidation in carbonate-buffered solution: 1. Experimental kinetics. Geochim. Cosmochim. Acta 52 (1077-1085).

Parisi, D., Horneman, J., Rastogi, V. (1994). Use of bactericides to control acid mine drainage. OSMRE Dir. TSR-10, U.S. OSMRE, Washington, D.C.

Park, I., Tabelin, C.B., Magaribuchi, K., Seno, K., Ito, M., Hiroyoshi, N. (2018a). Suppression of the release of arsenic from arsenopyrite by carrier-microencapsulation using Ti-catechol complex. J. Hazard. Mater. 344 (322-332).

Park, I., Tabelin, C.B., Seno, K., Jeon, S., Ito, M., Hiroyoshi, N. (2018b). Simultaneous suppression of acid mine drainage formation and arsenic release by Carrier-microencapsulation using aluminum-catecholate complexes. Chemosphere. 205 (414-425).

Peppas, A., Komnitsas, K., Halikia, I. (2000). Use of organic covers for acid mine drainage control. Minerals Engineering. 13, 5 (563e74).

Pinto, E., Sigaud-kutner, T.C.S., Leitao, M.A.S., Okamoto, O.K., Morse, D., Celepicolo, P., (2003). Heavy metal-induced oxidative stress in algae, Journal of Phycology. 39 (1008-1018).

Riley, M., Daniel, R.S. (2009). Surface reactivity of pyrite and related sulfides. Surface Science Reports. (641-645).

Rossman, W., Wytovich, E., Seif, J.M. (1997). Abandoned Mines Pennsylvania's Single Biggest Water Pollution Problem. Water Pollution Problem. Pennsylvania Department of Environmental Protection, Rachel Carson State Office Building, 400 Market Street, Harrisburg, Pennsylvania17105: http://www.dep.state.pa.us/dep/deputate/minres/bamr/mining_012397.htm

Sam, R.I., Alonson, M.L., Bartolomé, L., Galdames, A., Goiti, E., Ocejo, M., Moragues, M., Alonso, R.M., Vilas, J.L. (2013). Relevance study of bare and coated zero-valent iron nanoparticles for lindane degradation from its by-product monitorization, Chemosphere. 93 (1324-1332).

Sasaki, A. and Igarashi, T. (2013). Groundwater flow and chemistry around the tailing dam of a closed mine and countermeasures for the leachate. The 7th International Conference on Earth Resources Technology. November 11-13, 2013, Chiang Mai, Thailand.

Schweigert, N., Zehnder, A.J.B., Eggen, E.I.L. (2001). Chemical properties of catechols and their molecular modes of toxic action in cells, from microorganisms to mammals. J. Environ. Microbiol. 3, (81-91).

Shi, L.N., Zhang, X., Chen, Z.L. (2011). Removal of chromium (VI) from wastewater using bentonite-supported nano zero-valent iron, water. Res. 45, (886-892).

Shi, J., Yi, S., He, H., Long, C., Li, A. (2013). Preparation of nanoscale zero-valent iron supported on chelating resin with nitrogen doner atoms for simultaneous reduction of Pb2+ and NO3-, Chem. Eng., J. 230, (166-172).

Singer, P.C. and Stumm, W. (1968). Kinetics of the oxidation of ferrous iron. P. 12-34. In: 2nd Symp. On Coal Mine Drainage Research. Bituminous Coal Research, Inc., Monroeville, P.A.

Skousen, J.G., Faulkner, B.B., Sterner, P. (1995). Passive treatment systems and improvement of water quality. In: Processing, Fifteenth Annual West Virginia Surface Mine Drainage Task Forces Symposium, 4-5 April 1995, West Virginia University, Morgantown, WV.

Smith, E.E. and Shumate, K.S. (1970). Sulfide to sulfate reaction mechanism. Water pollution control Res. Series 14010 FPS. USDI, FWQA. Washington, D.C.

St-Germain, O., Larratt and Prairie, (1997). Field studies of biologically supported water covers at two Noranda tailing ponds. In: Processing of the fourth international conference on acid rock drainage, Vancover, British, Columbia, Canada, May 1997, Vol. 1 (131-148).

Stumm, W., Morgan, J.J. Aquatic Chemistry: An Introduction Emphasizing Chemical Equilibria in Natural Waters. New York 7 Wiley; 1981 (780).

Stark, L.R., Williams, F.M., Stevevens, S.E., Eddy, D.P. (1994). Retention and vegetative cover at the Simco constructed wetland: an appraisal through year eight of operation. P. 89-98. In: Internation land reclamation and mine drainage conference, 24-29 April 1994, USDI, Bureau of Mine SP 06A-94. Pittsburgh, PA.

Stark, L.R., William, F.M., Wenerick, W.R., Wuest, P.J. Urban, C.A. (1996). The effect of substrate type, surface water depth, and flow rate on manganese retention mesocosm wetland. J. Environ. Qual. 25 (97-106).

Suzuki, T., Moribe, M., Oyama, Y., Niinae, M. (2012). Mechanism of nitrate reduction by zero-valent iron: equilibrium and kinetics studies, Chem. Eng. J. 183, (271-277).

Tseng, H.H., Su, J.G., Liang, C. (2011). Synthesis granular activated carbon/zero valent iron composites for simulations adsorption/dichlorination of trichlorothylene, J. Hazard. Mater. 192 (500-506).

United States Environmental Protection Agency. (1997), A citizen's Handbook to Address Contaminated Coal Mine Drainage (EPA-903-K-97-003). United States Environmental Protection Agency, Cincinnati, OH.

Watson, A. (1995). Practical engineering options to minimize AMD potential. Second Australia AMD workshop proceeding. Ed: N.J. Grundon and L.C. Bell. Charters Towers, Queensland, Australia. 28-31 March. (53-67).

Wei, Y.T., Wu, S.C., Yang, S.W., Che, C.H., Lien, H.L., Huang, D.H. (2012). Biodegradable surfactant stabilized nanoscale zero-valent iron for in situ treatment of vinylchoride and 1,2 - dichloroethane, J. Hazard. Mater.211-212 (373-380).

Xiao, S.L., Ma, H., Shen, M.W., Wang, S.Y., Haung, Q.G., Shi, X.Y. (2011). Element copper(II) removal using zero-valent iron nanoparticle-imobilized hybrid electrospun polymer nonofibrous mats, Colloids Surf. A 281 (48-54).

Yanful, E. and Nicholson, R. (1991). Engineering soil covers for reactive tailing management: Theoretical concepts and laboratory development. In: Proceeding of the second international conference on the Abatement of acid drainage, vol.1, pp. 461-487. September 16-18, 1991, Montreal, PQ Canada.

Yin, Y., Wu, J., Li, P., Wang, X., Zho, N., Wu, P., Yang, B. (2012). Experimental study of zero-valent iron induced nitrobenzene reduction in groundwater: the effect of pH, iron dosage, oxygen and comment dissolved anions. Chem.Eng. J. 184 (198-204).

Younger, P. L. (2000). Holistic remedial strategies for short and long-term water pollution from abandoned mines. Transaction of the Institution of Mining and metallurgy (section A: Mining technology), 109: A210-A218.

Zhang, X., Deng, B., Guo, J., Wang, y., Lan, Y. (2013). Ligand-assisted degradation of carbon tetrachloride by microscale zero-valent iron. J. Environ. Manage. 92 (1328-1333).

CHAPTER 2: GALVANIC MICROENCAPSULATION (GME) USING ZERO-VALENT IRON TO SUPPRESS PYRITE OXIDATION

2.1 Introduction

A large amount of waste is generated from mining activities that contain sulfide minerals such as pyrite (FeS_2) (Tabelin et al., 2018). More recently, pyrite-rich debris is also excavated during underground and tunnel construction projects in exceptionally large amounts (Tabelin et al., 2010, 2012a, 2012b, 2014a, 2014b, 2017a, 2017b, Tamoto et al., 2015). When sulfide minerals like pyrite are exposed to the environment, acid mine drainage (AMD) is usually generated. AMD is very acidic (pH<3) and contains high concentrations of hazardous heavy metals such as copper (Cu), lead (Pb), and zinc (Zn) as well as toxic metalloids like arsenic (As) and selenium (Se) (Akcil et al., 2006, Barrie et al., 2005, Elsetinow et al., 2001, Evangelou et al., 2001, Moodley et al., 2017, Sheoran, et al., 2006, Tabelin et al., 2012c, 2012d, 2013, Tatsuhara et al., 2012, Yuting et al., 2015). Eq. 2.1 shows the initial oxidative dissolution of pyrite by dissolved oxygen (DO) and as this process continues, more ferrous ions (Fe^{2+}) are generated while the pH becomes more acidic. Eq. 2.2 shows the oxidation reaction of Fe^{2+} with DO to form ferric ions (Fe^{3+}), a strong oxidant that could enhance the oxidization of pyrite and promote AMD formation (Eq. 2.3).

$$FeS_{2(s)} + 3.5\ O_2 + H_2O = Fe^{2+}{}_{(aq)} + 2\ SO_4{}^{2-}{}_{(aq)} + 2\ H^+{}_{(aq)} \quad (2.1)$$

$$Fe^{2+}{}_{(aq)} + 0.25\ O_{2\,(aq)} + H^+{}_{(aq)} = Fe^{3+}{}_{(aq)} + 0.5\ H_2O \quad (2.2)$$

$$FeS_{2(s)} + 14\ Fe^{3+}{}_{(aq)} + 8\ H_2O = 15\ Fe^{2+}{}_{(aq)} + 2\ SO_4{}^{2-}{}_{(aq)} + 16\ H^+{}_{(aq)} \quad (2.3)$$

The most widely used technique to mitigate the negative environmental impacts of AMD is via neutralization. In this technique, basic materials such as limestone are added to AMD to increase its pH and precipitate most of the heavy metals as metal oxyhydroxides (Demers et al., 2015, Heviánková et al, 2013, Kleinmann et al., 1998). Even though this technique is effective, AMD generation could continue for several decades or even centuries, so this approach is unsustainable. Microencapsulation is a promising and potentially more sustainable approach because it limits AMD production by suppressing pyrite oxidation directly through the formation of a passivating coating on the mineral. The first encapsulation technique was developed by Evangelou (2001) by forming ferric phosphate coating on pyrite surface. The author use was using hydrogen peroxide (H_2O_2) to oxidize Fe^{2+} to Fe^{3+}. However, in the real plant H_2O_2 could not target

pyrite and it is very difficult to handling. Carrier microencapsulation (CME), a microencapsulation technique developed by Satur et al. (2007), uses redox-sensitive metal(loid)-organic complexes to carry the coating material to the surface of pyrite where the complexes are adsorbed and decomposed, releasing the insoluble metal(loid) ion of the complex that is rapidly precipitated to form a protective coating on pyrite. Because pyrite dissolves via an electrochemical mechanism, the redox-sensitive metal(loid)-organic complexes have been shown to selectively target pyrite even in a complex system containing arsenopyrite, pyrite, and quartz (Park et al., 2018a, b). One current limitation of this technique is the use of catechol, which when oxidized in the presence of DO and metal ions like Fe^{3+} and Cu^{2+}, forms semiquinone radicals, superoxides, and H_2O_2 that are toxic to cells (Schweigert et al., 2001).

Another way to selectively target pyrite in a complex system is via galvanic interaction, which occurs when two semiconductive or conductive materials having different rest potentials come in close contact with each other. In this process, material having a lower rest potential becomes the anode and is dissolved while the other material with higher rest potential becomes the cathode and is galvanically protected (Akcil et al., 2006, Brett et al., 1993, Evangelou, 2001, Greet et al., 2004, Huang et al., 2005, Martin et al., 1991, Subrahmanyam and Forssberg, 1993, Yufan et al., 2018). Using this concept, we developed a new technique to suppress pyrite oxidation called galvanic microencapsulation (GME). In this technique, there are two reactions that would potentially suppress pyrite oxidation: (1) sacrificial effect of the anode, and (2) coating formation using the oxidation products from the anode. GME, similar to CME, would be selective because pyrite oxidation is an electrochemical process and GME involves electron transfer between anodic and cathodic sites. Zero-valent aluminum (ZVAl) and zero-valent iron (ZVI) are potentially good candidates as anodes for this technique because both metals have lower redox potentials (ZVAl = -1.67 V and ZVI = -0.44 V) than pyrite (+0.2 to +0.3 V). Moreover, ZVAl and ZVI are non-toxic and these materials often end up as wastes, so they are easily obtainable. In this chapter, galvanic interactions of pyrite with ZVAl or ZVI under various conditions are investigated. Specifically, this it aims to: (1) elucidate the effects on pyrite oxidation of ZVAl or ZVI dosage, leaching time, and pH, (2) understand the suppression mechanisms during GME, and (3) improve coating formation and coverage using phosphate. These objectives were achieved by conducting batch leaching experiments, geochemical modeling, and electrochemical studies like cyclic voltammetry (CV) and chronoamperometry. The surface characteristics of ZVAl and ZVI samples, as well as the leaching residues, were also analyzed by scanning electron microscopy with energy dispersive X-ray spectroscopy (SEM-EDX) and diffuse reflectance infrared Fourier

transform spectroscopy (DRIFTS) to understand changes in the pyrite oxidation products in the presence of ZVAl and ZVI.

2.2 Materials and methods

2.2.1 Materials

The pyrite sample used in this study was obtained from Huanzala Mine, Huanuco, Peru. The X-ray diffraction (XRD) pattern shows that it is mainly composed of pyrite and contains Fe (44.6%) and S (54.3%) as the main components with only trace impurities like calcium (0.36%), silicon (0.32%) and aluminum (0.15%) (Figs. 2.1a & b). Pyrite was crushed by a jaw crusher, ground with a ball mill, and sieved to obtain a size fraction of 500-710 μm. Ultra-pure ZVAl and ZVI (99.9%) used in this study were obtained from Wako Pure Chemical Industries Ltd., Japan, and Figs. 2.1c & d show their particle size distributions, which were measured by LASER diffraction (Microtrac® MT3300SX, Nikkiso Co. Ltd., Japan). The D_{50} of ZVAl and ZVI were similar at around 25 μm.

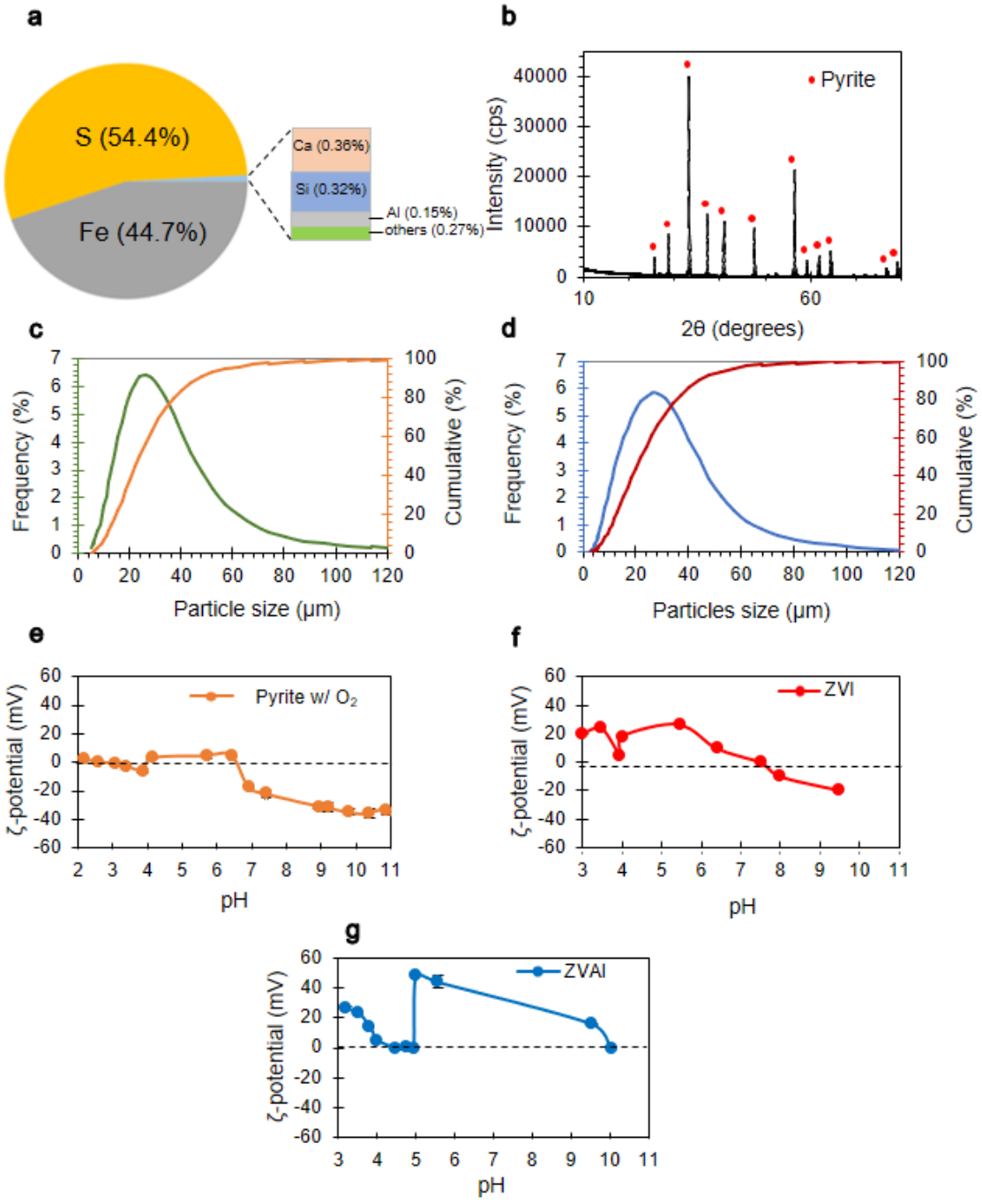

Fig. 2.1 (a) Chemical composition of pyrite sample, (b) XRD pattern of pyrite sample, (c) particle size distribution of ZVAl, (d) particle size distribution of ZVI, (e) zeta potential distribution of pyrite with pH under oxic (with O_2) condition, and (f) & (g) zeta potential distribution of ZVI and ZVAl with pH under oxic (with O_2) condition, respectively.

2.2.2 Leaching experiments and chemical analysis

Before the leaching experiments, the pyrite sample (500-700 μm) was washed using the method described by McKibben and Barnes (1986) to remove any oxidized layer formed during sample preparation and storage. Leaching experiments were conducted by mixing 1 g of washed pyrite, 10 mL of deionized (DI) water, and predetermined amounts of ZVAl or ZVI in an Erlenmeyer flask. For the experiments with various dosages and pH, the shaking time was fixed to 3 days while in the leaching experiments with time, the dosage of ZVAl or ZVI was fixed at 0.1 g without any pH adjustments. The flasks were shaken (shaking amplitude and rate of 40 mm and 120 strokes/min, respectively) in a constant temperature water bath shaker (25 ºC). After the predetermined leaching time, the flasks were removed from the shaker, the pH and redox potential (Eh) of suspensions were measured, and the leachates were collected by filtration through 0.2 μm syringe-driven membrane filters (Sartorius AG, Germany). The concentrations of total S as SO_4^{2-} (dissolved S), dissolved Fe, and dissolved Al in the filtrates were analyzed by inductively coupled plasma atomic emission spectroscopy (ICP-AES, ICPE-9820, Shimadzu Corporation, Japan) (margin of error ± 2%). Meanwhile, the residues were washed thoroughly with DI water and dried in a vacuum drying oven at 40 ºC for 24 hours. The residues were analyzed using a high-magnification optical microscope (VHX-1000, Keyence Corporation, Japan), SEM-EDX (SSX-550, Shimadzu Corporation, Japan), and ATR-FTIR (FT/IR-6200HFV and ATR Pro One attachment equipped with a diamond prism, Jasco Analytical Instruments, Japan). Some of the leaching experiments were done in triplicates to ascertain that the observed trends were statistically significant.

2.2.3 Electrode preparation and electrochemical measurements

The pyrite electrode was prepared by cutting a small cuboid from a large pyrite crystal, placing it in the center of PVC rings, connecting the crystal to Cu wires using a silver conducting paste, and fixing it in place using a non-conductive resin (Technovit®, Heraeus Kulzer GmbH, Germany). The pyrite electrode was polished using sandpapers of decreasing grit size (#400, #600, #800, #1500, and #2000) and then smoothened by polishing with 5 and 1 μm alumina paste on a smooth glass plate. The pyrite electrode was then ultrasonically cleaned for 5 min to remove any residual alumina particles and washed thoroughly with DI water.

For the electrochemical measurements, a conventional three-electrode system attached to an electrochemical measurement unit (SI 1280B, Solartron Instruments, UK) was used. For the electrochemical setup, pyrite was the working electrode, platinum was the counter electrode and

Ag/AgCl in saturated KCl solution was the reference electrode. In the electrochemical measurements, pyrite electrode with and without ZVAl and ZVI were measured by CV and chronoamperometry. The pyrite electrode with ZVAl and ZVI was prepared as follows: (1) ZVAl or ZVI was suspended in acetone, and (2) the suspension was put on the surface of the polished pyrite electrode. After the evaporation of acetone, pyrite with ZVAl or ZVI was used as the working electrode.

All CV measurements were carried out (in 0.1M Na_2SO_4 solution as supporting electrolyte) at 25 °C under a nitrogen (N_2) atmosphere. The CV measurements started after equilibration at the open circuit potential (OCP) and the sweep direction was towards more positive potentials first (+0.8 V vs. Ag/AgCl) (i.e., anodic direction) at a scan rate of 30 mV/s for 5 cycles.

Chronoamperometry is an electrochemical technique wherein a fixed potential is applied to the working electrode and changes in the current density are recorded with time. By applying a fixed potential to the pyrite electrode, the anodic and cathodic half-cell reactions during pyrite oxidation could be decoupled and elucidated independently for a prolonged period of time. The chronoamperometry measurements were conducted using the same setup as the CV measurements but with magnetic stirring at 250 rpm. For the anodic polarization measurements, the pyrite electrode was first equilibrated at the OCP, and then anodically polarized at +0.6 V vs. Ag/AgCl for 4.5 hours under N_2 atmosphere. Similarly, the cathodic polarization experiments were conducted using a similar setup as the anodic polarization but at an applied potential of -0.2 V vs. Ag/AgCl, and without N_2 purging. These applied potentials were selected based on the previous studies of Kelsall et al. (1999) and Tabelin et al. (2017c, d).

2.3 Results and discussion

2.3.1 Effects of the presence ZVAl or ZVI on pyrite oxidation with time and pH

2.3.1.1 Effects of ZVAl or ZVI dosage

Fig. 2.2 shows the final pH and dissolved S, Fe, and Al concentrations of the leachates after 3 days of leaching with various amounts of ZVAl or ZVI in DI water. Fig. 2.2a illustrates that dissolved S concentration decreased as the dosage of ZVAl or ZVI increased, which suggest that both ZVAl and ZVI suppressed the oxidation of pyrite. The initial pH of the control (i.e., pyrite and DI water only) was around 5.6 but decreased to pH 4 after 3 days of leaching due to pyrite oxidation (Eq. 2.2 & 2.3) (Park et al. 2018b; Tabelin et al. 2017c). In the presence of ZVI, higher dosage caused the pH to increase coincident with lower dissolved Fe concentration due to the

enhanced precipitation of dissolved Fe at high pH values. The increase in pH in the presence of ZVI could be attributed to the reaction of ZVI with water and DO producing OH^-, which leads to the increase in pH (Eq. 2.4). Previous studies have shown that higher pH values enhanced pyrite oxidation (Ahlberg et al., 1990; Mckibben et al., 1986; Moses et al., 1990; Tabelin and Igarashi, 2009), but when ZVI was added into the solution, the dissolved S concentration was low even at higher pH values. There are two possible explanation for this observed discrepancy: (1) oxidation of ZVI consumed DO and the low DO concentration limited pyrite oxidation, and (2) galvanic interaction between pyrite and ZVI suppressed pyrite oxidation.

$$2Fe^0\,(s) + O_2 + 2\,H_2O = 2Fe^{2+} + 2\,OH^- \qquad (2.4)$$

The consumption of DO by ZVI was determined by directly measuring the decrease of DO concentration with a DO meter and the results showed that 1 g of ZVI consumed only around 20% of DO (Eq. 2.4 & Fig. 2.3). This implies that the slightly lower DO concentration was not the main cause of the suppression of pyrite oxidation. The second possibility will be explained in more detail in the next subsection using electrochemical techniques. Higher dosage of ZVAl also resulted in the decrease of dissolved S and Fe concentrations as illustrated in Figs. 2.2a & c while dissolved Al was detected due to the dissolution of ZVAl (Eq. 2.5). In contrast to ZVI, ZVAl addition had negligible effects on the pH. There are two possible explanation for the lower dissolved S and Fe concentrations in the presence of ZVAl. Firstly, dissolved S and Fe could be co-precipitated with dissolved Al via the formation of hydrobasaluminite ($Al_4(SO_4)(OH)_{10}\cdot nH_2O$) and schwertmannite ($Fe_8O_8(SO_4)_y(OH)_x$). According to Sánchez-España et al. (2011, 2016), these two phases could be precipitated at around pH 4, sequestering dissolved Al, Fe, and S from solution. Based on our thermodynamic calculations, saturation indices of these two precursor minerals were positive, which suggest that their precipitation during the experiments were thermodynamically favorable (Table 2.1). Secondly, the lower dissolved S and Fe could be attributed to the suppression of pyrite oxidation via galvanic effect and will be explained in detail in the next subsection. Although an increase in pH should occur in the presence of ZVAl as explained by Eq. 2.5, Fig. 2.2b illustrates that there was insignificant change in pH after the leaching experiments even at very high ZVAl dosages. This almost constant pH at high ZVAl dosages could be explained by (Eqs. 2.6 & 2.7). Although, the oxidation of ZVAl in water releases OH^- (Eq. 2.6), this alkalinity it is neutralized by the H^+ released by the precipitation of

hydrobasaluminite and schwertmannite (Eq. 2.7), which balances the pH of the solution. Comparing the two metals, dissolved S concentration with ZVI was lower than that with ZVAl.

$$2Al^0 + 1.5\ O_2 + 3\ H_2O = 2\ Al^{3+} + 6\ OH^- \quad (2.5)$$

$$4\ Al_3^+ + SO_4^{3-} + 14\ H_2O = Al_4(SO_4)(OH)_{10} \cdot 4H_20 + 10H^+ \quad (2.6)$$

$$8\ Fe^{3+} + y\ SO_4^{2-} + (24 - 2y + x)/\ 2\ H_2O = Fe_8O_8(SO_4)_y(OH)_x + (24 - 2y)\ H^+ \quad (2.7)$$

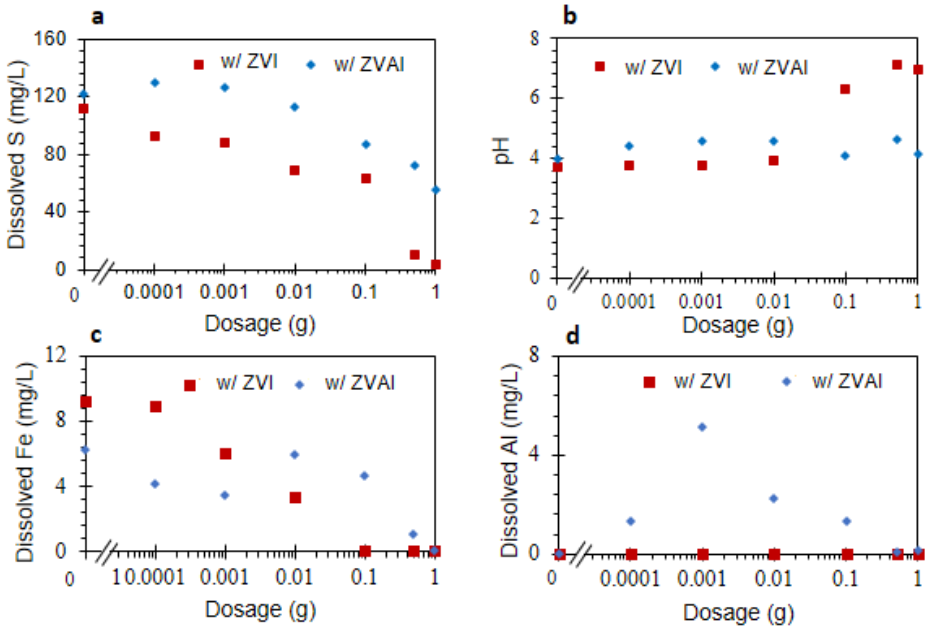

Fig. 2.2 Leaching of pyrite with various dosage of ZVAl or ZVI: (a) dissolved S concentration after leaching, (b) pH of the solution after leaching, (c) dissolved Fe concentration after leaching, and (d) dissolved Al concentration after leaching.

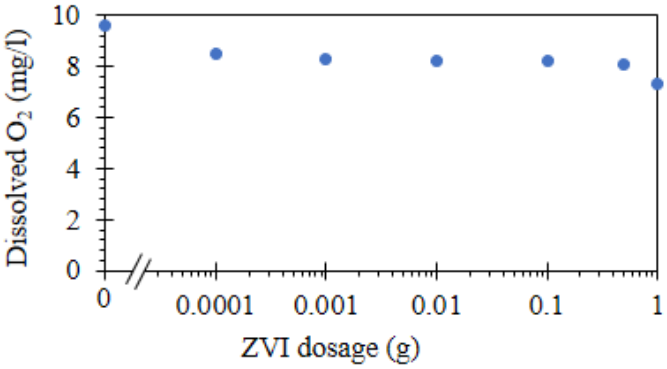

Fig. 2.3 Dissolved O_2 with various ZVI dosages.

Table 2.1 Saturation indices of hydrobasaluminite and schwertmannite based on the experimental results

Mineral	**Saturation Index (SI)**
Hydrobasaluminite	2.3
Schwertmannite	0.88

2.3.1.2 Effects of the presence of ZVAl or ZVI on pyrite oxidation with time

Fig. 2.4 shows the changes of pH, dissolved S, and dissolved Fe with time in the presence of ZVAl or ZVI up to 21 days. When ZVAl was added, the concentration of dissolved S slightly decreased compared with the control but was statistically insignificant especially in the first 3 days. In comparison, dissolved S in the presence of ZVI was relatively lower than the control in the same period, which could be attributed to the suppression of pyrite oxidation via galvanic interactions. The better suppressive effects of ZVI compared to ZVAl could be explained by two possibilities: (1) ZVI is positively charged while pyrite is negatively charged at pH values less than 7.5 (Figs. 2.1e & g), which makes it easier for them to come in contact via electrostatic attraction, and (2) at higher pH, dissolved Fe generated from ZVI reaction with oxygenated water was precipitated as iron-oxyhydroxide/oxide on pyrite that inhibited pyrite oxidation. After 7 days, however, the suppressive effects of ZVI on pyrite oxidation disappeared as illustrated in the similar dissolved S concentrations of the control and that with ZVI. In the presence of ZVI, the pH was buffered at around 7 for 7 days, but in the control, the pH decreased from 5.8 to 3.5. The higher pH in the case with ZVI likely enhanced the precipitation of dissolved Fe via two

mechanisms: (1) direct precipitation of Fe^{2+} to $Fe(OH)_2$ (Eq. 2.8), and (2) Fe^{2+} was oxidized to Fe^{3+} and then precipitated as $Fe(OH)_3$ (Eq. 2.9). With time, the Fe^{2+}-precipitates formed via mechanism (1) could also be oxidized by oxygen to $Fe(OH)_3$ based on (Eq. 2.10) and by catalysis reaction with ZVI (Jones et al., 2014, Wehrli et al., 1989). Compared to the experiments with ZVI, dissolved Fe concentrations in the control were higher because at around pH 3.5, direct precipitation of Fe^{2+} and the oxidation of Fe^{2+} to Fe^{3+} by DO become negligible and sluggish, respectively (Lowson et al.,1982, Singer and Stum, 1970, Stumm and Lee, 1961).

$$Fe^{2+} + 2H_2O = Fe(OH)_2 + 2H^+ \quad (2.8)$$

$$Fe^{3+} + 3H_2O = Fe(OH)_3 + 3H^+ \quad (2.9)$$

$$2Fe(OH)_2 + 0.5O_2 + 2H_2O = 2Fe(OH)_3 + H_2O \quad (2.10)$$

Although dissolved Fe was precipitated in the case with ZVI, SEM-EDX observations of leaching residues after 3 days show that the pyrite surface was not covered by Fe-oxyhydroxide precipitates (Fig. 2.5). This means that dissolved Fe was precipitated only in the solution, but this precipitate did not attach onto pyrite because based on the zeta potential measurements, oxidized pyrite at pH 4-6 is positively charged similar to that of Fe-oxyhydroxides/oxides (Figs. 2.4e & f). These results suggest that under the conditions of our experiments, attachment of precipitated Fe-oxyhydroxides onto pyrite was unfavorable, so coating formation was negligible.

In contrast, the suppressive effects of ZVAl on pyrite oxidation in the first 3 days were negligible. After 7 days, however, the leaching concentration of dissolved S became lower than the control. When ZVAl is present with pyrite, galvanic interactions should occur as shown in Eq. 2.5 that would suppress pyrite oxidation. However, ZVAl is covered by a thin oxyhydroxide film (Fig. 2.4a), so galvanic interaction was limited. After 3 days, the pH of suspension became slightly acidic (pH<4) that enhanced the dissolution of the oxyhydroxide film on ZVAl (Fig. 2.4a), which promoted galvanic interactions and suppressed pyrite oxidation. The results showed that ZVAl could continue to suppress pyrite oxidation (up to 21 days) provided that it is not passivated by Al-oxyhydroxides (e.g., under acidic conditions).

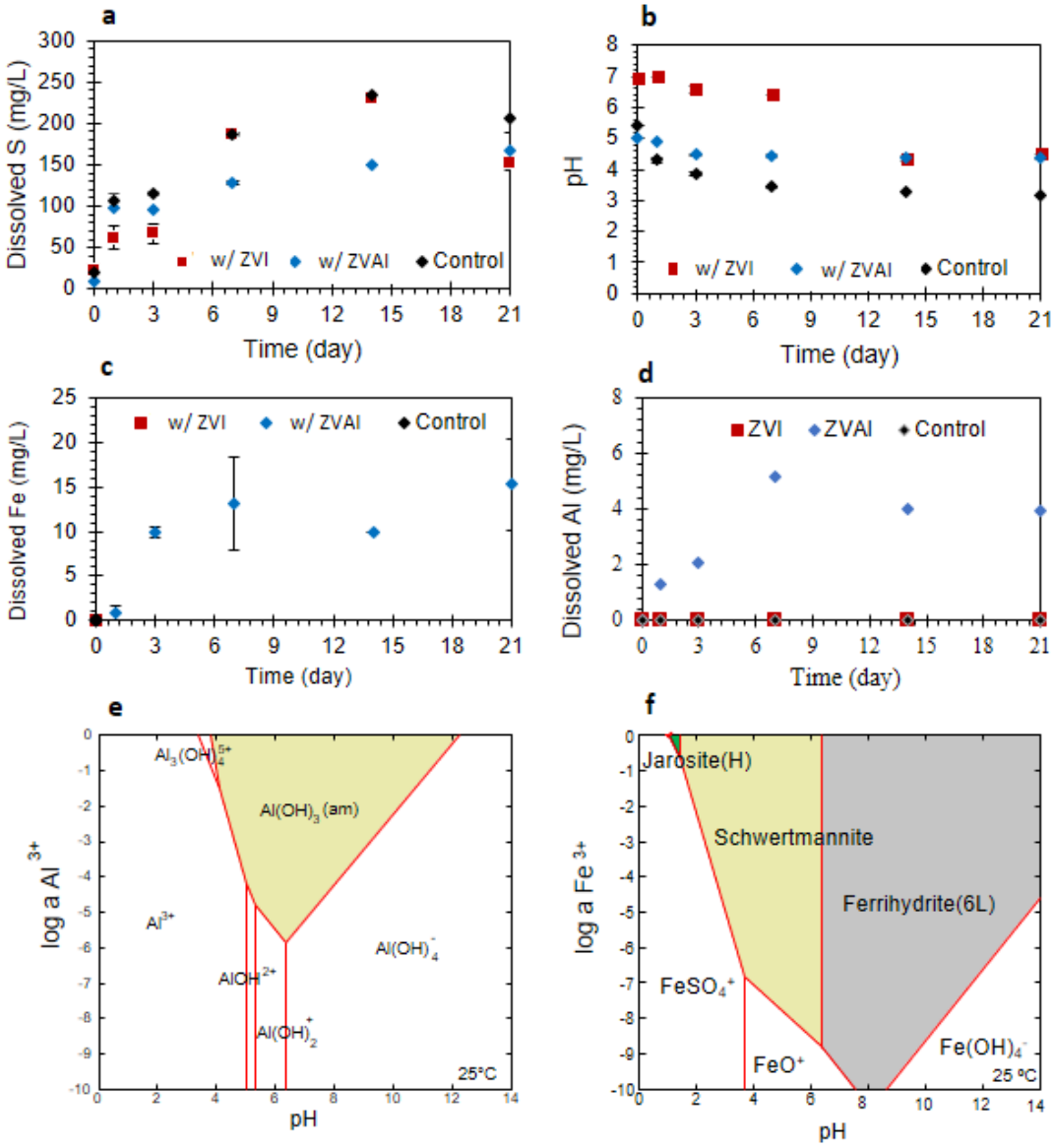

Fig. 2.4 Leaching result of pyrite in the presence of ZVAl or ZVI with time and the equilibrium log a-pH diagram of Al^{3+} and Fe^{3+} : (a) dissolved S concentration change with time, (b) pH change with time, (c) dissolved Fe concentration change with time, (d) dissolved Al concentration change with time, (e) log *a*-pH predominance diagram of Fe^{3+} at 25 ºC, 1.013 bars, and activity of SO_4^{3-} = 10^{-3}, and (f) log *a*-pH predominance diagram of Al^{3+} at 25 ºC, 1.013 bars, and activity of SO_4^{3-} = 10^{-3}.

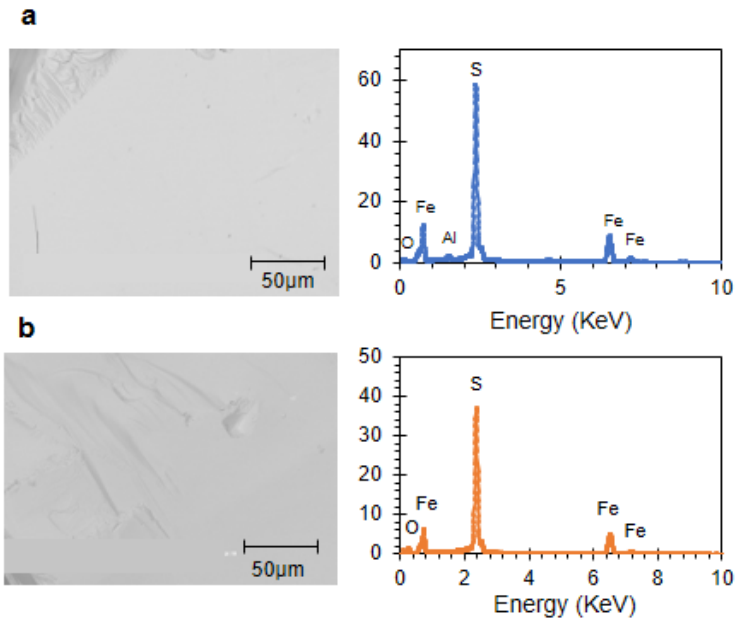

Fig. 2.5 SEM-EDX of pyrite after leaching with ZVAl or ZVI: (a) leaching with ZVAl for 3 days, and (b) leaching with ZVI for 3 days.

2.3.1.3 Effects of the presence of ZVI on pyrite oxidation with pH

As described previously, pH is an important parameter during pyrite oxidation, but because the presence of ZVI strongly affected this parameter, the effects of ZVI on pyrite oxidation remain unclear. In this subsection, the effects of initial pH were investigated using DI (pH 5.8), 0.01M HCl (pH 2), and 0.001M NaOH (pH 11). Fig. 2.6 shows the changes in pH, dissolved S, and dissolved Fe with time. In the presence of ZVI, the pH in the three solutions increased as follows: from 5.8 to 7 in DI water, from 2 to 6.2 in 0.01M HCl, and from 9 to 10 in 0.001M NaOH. This initial increase in pH could be attributed to the pH buffering effects of ZVI as discussed previously. It is interesting to note that the initial pH buffering effects of ZVI became smaller as the pH becomes more alkaline; that is the buffering effects of ZVI in the 0.001M NaOH were negligible compared with that in DI water. At higher pH, ZVI becomes coated with an Fe-oxyhydroxide film that limited its suppressive effects on pyrite oxidation via galvanic interaction, so the pH decreased with time due to pyrite oxidation. In the case of 0.01M HCl, the pH rapidly decreased due to the precipitation of Fe^{3+} (Eq. 2.8) generated from the gradual oxidation of Fe^{2+} from ZVI. Dissolved S concentrations were dramatically lower in the 0.01M HCl solution until 21 days, indicating that suppression of pyrite oxidation by ZVI via galvanic interaction was most effective

under acidic conditions. The strong suppressive effects of ZVI on pyrite oxidation under acidic conditions could be attributed to two reasons: (1) ZVI is positively charged while pyrite is negatively charged at pH values between 3 and 4 (Figs. 2.4 e&g), which makes it easier for them to come in contact via electrostatic attraction, and (2) Fe-oxyhydroxide/oxide layer on ZVI, which could inhibit the transfer of electrons, was most likely not formed (Moses et al., 1987, Schwertmann and Cornell, 2003).

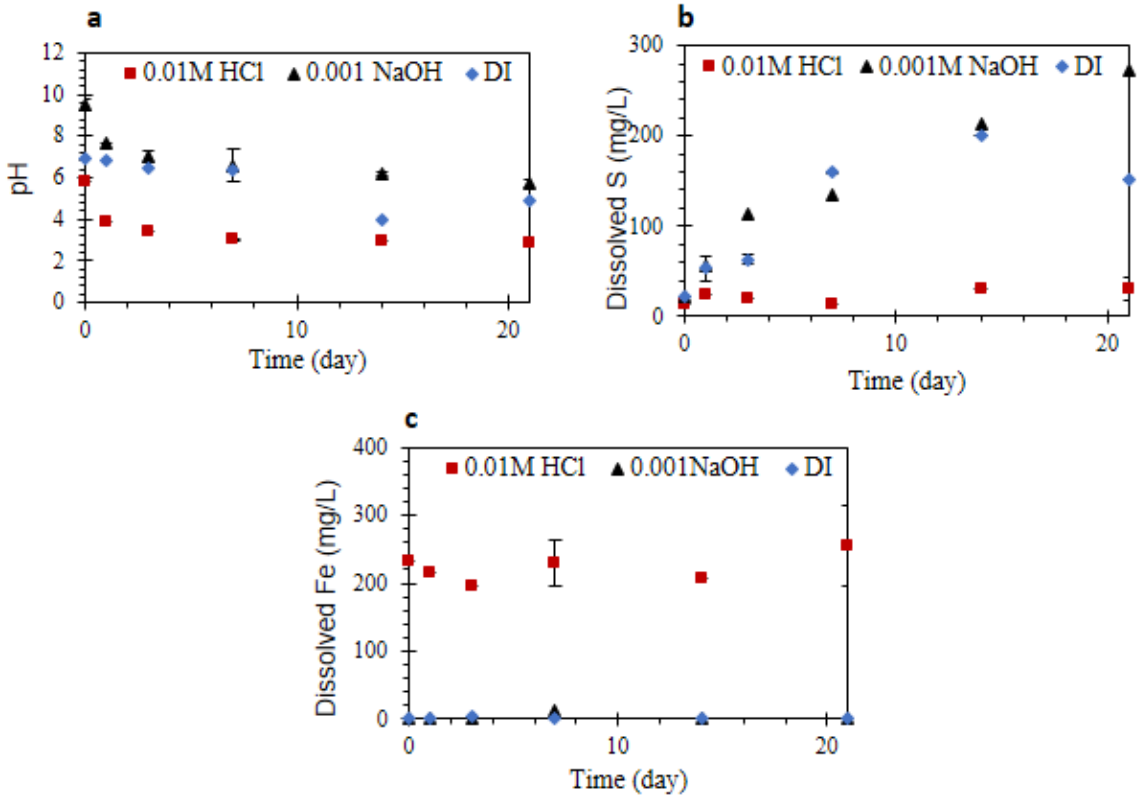

Fig. 2.6 Evolution of leachate chemistry in deionized (DI water), 0.01M HCl, and 0.001M NaOH as well as the zeta-potential distributions of pyrite and ZVI with pH: (a) pH change with time (b) dissolved S concentration change with time, and (c) dissolved Fe concentration change with time.

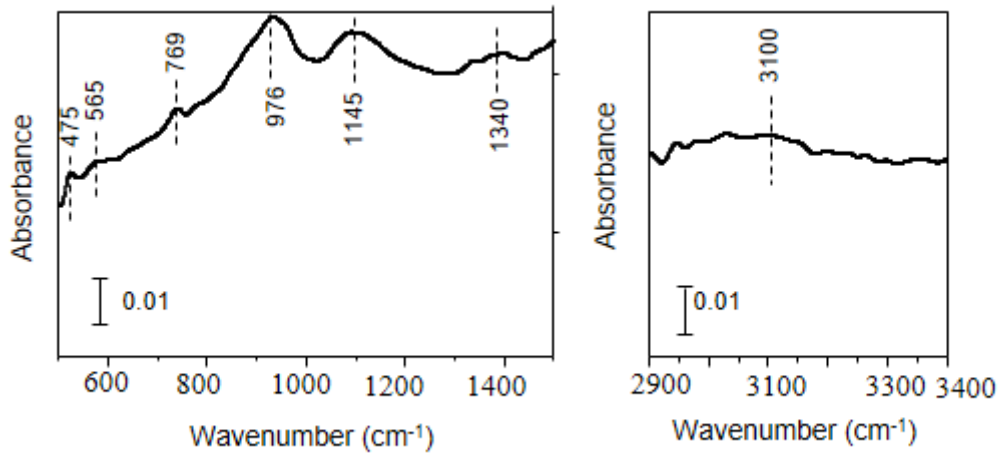

Fig. 2.7 ATR-FTIR spectrum of ZVAl used in the experiment.

2.3.2 Electrochemical studies

2.3.2.1 Cyclic voltammetry and chronoamperometry measurements of pyrite electrode with ZVAl

To confirm that the suppression of pyrite oxidation was primarily due to galvanic interaction between pyrite and ZVAl or ZVI, electrochemical studies were conducted. Fig. 2.8 shows the first CV cycles of pyrite with and without attached ZVAl. The OCP measured in the case without ZVAl on the pyrite electrode (i.e., freshly polished surface) was +0.2 V but with ZVAl, the OCP shifted to a more negative value (-0.1 V). This OCP shift could be attributed to the effects of ZVAl on the surface of pyrite because partially oxidized ZVAl has an OCP of around -0.2 V, which was measured during our preliminary experiment. Although the OCP shifted with attached ZVAl, the current density profiles with and without ZVAl were similar. The duration of CV measurements is very short (one cycle = 107 s), so even though the CV results show that ZVAl only had minute effects for a short time, it might affect pyrite oxidation for longer periods of time as illustrated by the leaching results discussed previously (Fig. 2.4).

To evaluate the effects of ZVAl on pyrite oxidation for a longer period of time, chronoamperometry was conducted. Fig. 2.8b shows the changes in current density with time during the anodic polarization of pyrite with and without ZVAl at +0.6 V (Eq. 2.1). Initially, the current density of pyrite with ZVAl was similar to that without ZVAl and is consistent with the CV results. As discussed previously, ZVAl is very reactive, so an Al-oxyhydroxide film is easily formed on its surface. The presence of this film on the ZVAl sample used in this study was

confirmed by ATR-FTIR (Fig. 2.7). Al-oxyhydroxide is an insulating material, which might prevent the transfer of electrons, and could explain why the suppressive effects of ZVAl on pyrite oxidation in the first 3 days of leaching were negligible (Fig. 2.4). However, after about 500 seconds the current density of pyrite with ZVAl started to become higher than that without ZVAl, which continued until the end of the experiment. The higher current density could be explained by the galvanic interaction between ZVAl and pyrite after the dissolution of Al-oxyhydroxide layer on ZVAl with time at slightly acidic pH (electrolyte pH = 5.72) (Fig. 2.4f). This means that galvanic interaction between pyrite and ZVAl could occur when the Al-oxyhydroxide film on ZVAl is removed. Fig. 2.8c shows the changes in current density with time during the cathodic polarization of pyrite with and without ZVAl at -0.2 V. The current density of pyrite with ZVAl was smaller than that without ZVAl, which means that ZVAl suppressed the cathodic half-cell reaction of pyrite oxidation. When ZVAl particles cover the surface of pyrite, the cathodic sites are physically protected from oxidants and Eqs. 2.11 & 2.12 are suppressed.

$$FeS_2 + 8\ H_2O = Fe^{2+} + 2\ SO_4^{2-} + 16\ H^+ + 14e^- \quad (2.11)$$

$$O_2 + 4\ H^+ + 4\ e^- = 2\ H_2O \quad (2.12)$$

$$Fe^{3+} + e^- = Fe^{2+} \quad (2.13)$$

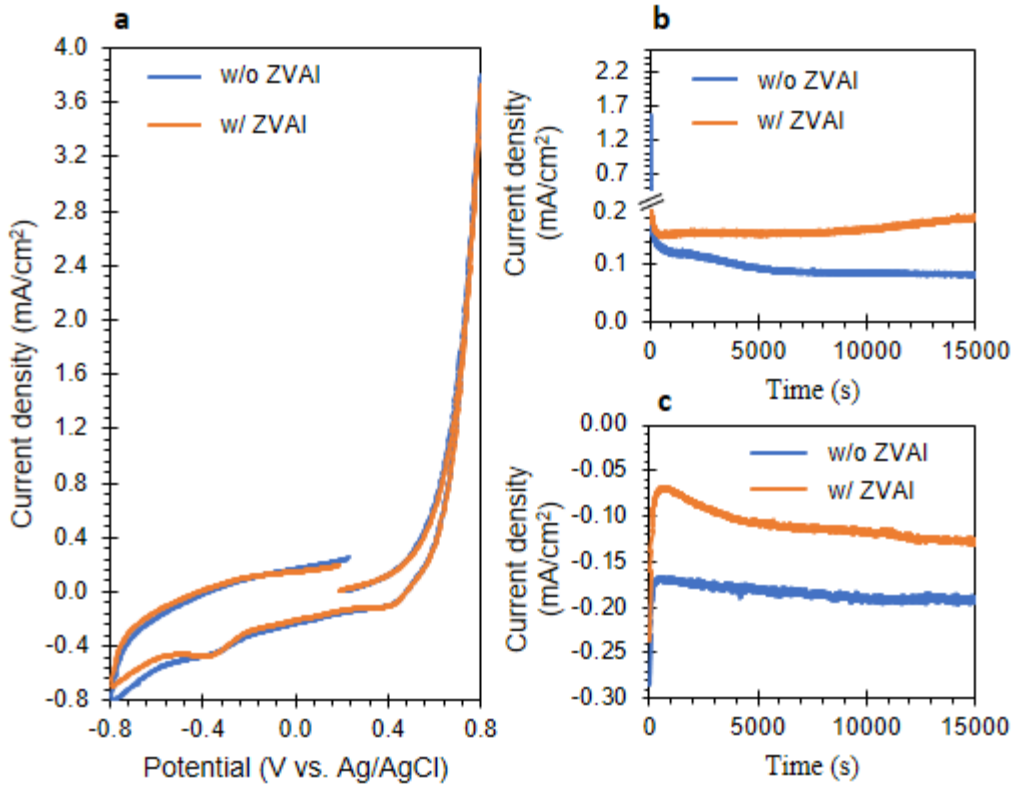

Fig. 2.8 Cyclic voltammetry and chronoamperometry of pyrite with and without attached ZVAl: (a) cyclic voltammetry of pyrite with and without attached ZVAl, (b) anodic polarization curves with time of pyrite with and without attached ZVAl, and (c) cathodic polarization curves with time of pyrite with and without attached ZVAl.

2.3.2.2 Cyclic voltammetry and chronoamperometry measurements of pyrite electrode with ZVI

Fig. 2.9 shows the first CV cycles of the pyrite electrode with and without attached ZVI. With attached ZVI, the current density was higher compared with that without ZVI (Fig. 2.9a-1), which could be attributed to the oxidation of ZVI on the pyrite surface (Eq. 2.4). In the cathodic sweep, the current density was smaller with attached ZVI than that without ZVI likely because ZVI limited the electron transfer to oxidants by physical protection (Fig. 2.9a-2) (Tabelin et al., 2017b).

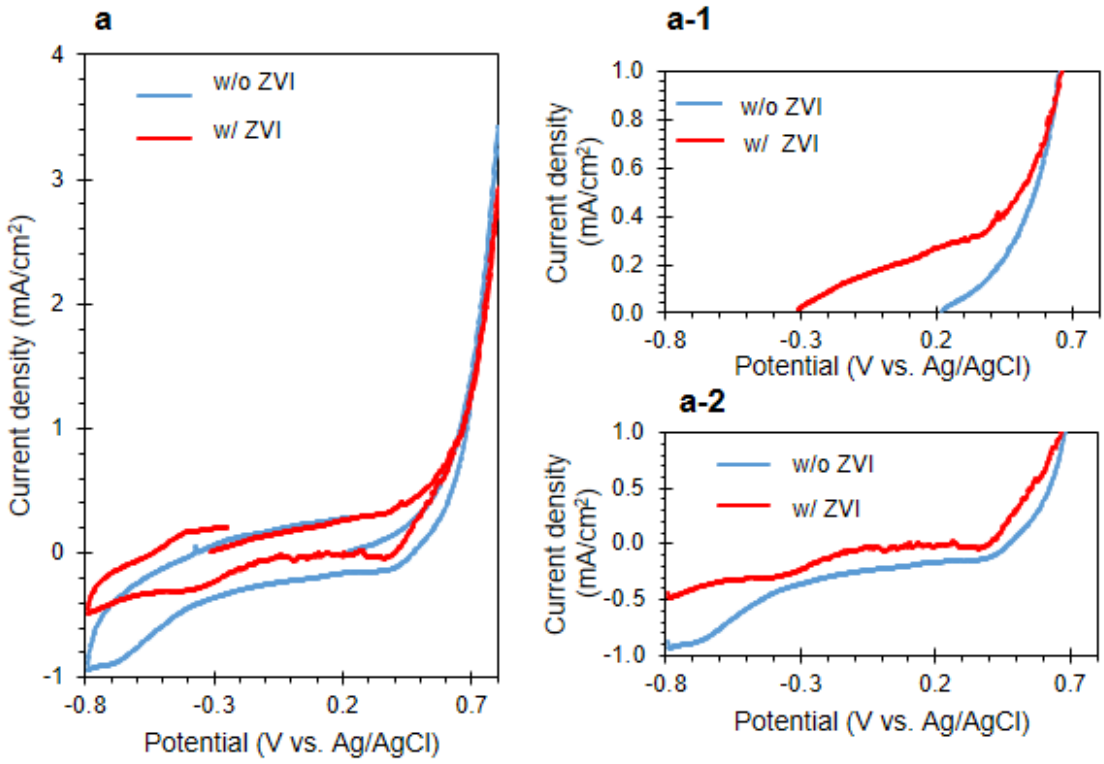

Fig. 2.9 Cyclic voltammetry of pyrite with and without attached with ZVI: (a-1) anodic sweep of the first cycle, and (a-2) cathodic sweep of the first cycle.

Figs. 2.10a & b show the anodic and cathodic polarization curves with and without ZVI on pyrite surface, respectively. In the presence of ZVI, the current density was larger than that without ZVI, and this trend continued until the end of the experiment. This higher current density with ZVI, which was also noted in the CV results, could be explained by the galvanic interaction between ZVI and pyrite; that is, when ZVI is in contact with pyrite under oxidizing conditions (i.e., positive Eh), it protects pyrite by acting as a sacrificial and is preferentially dissolved. It is also interesting to note that the oxidation of ZVI on the pyrite surface occurred quickly and continued for quite a long period of time (ca. 4.5 hours), which suggests that so long as conditions are slightly acidic, ZVI could protect pyrite under oxidizing conditions. These results further support our earlier deduction that the suppressive effects of ZVI on pyrite oxidation during the leaching experiments was largely due to galvanic interactions. Fig. 2.10b shows the changes in current density with time of pyrite with and without ZVI polarized at -0.2 V. The current density of pyrite with ZVI was smaller than that without ZVI, which means that ZVI suppressed the cathodic half-cell reaction of pyrite oxidation. When ZVI particles cover the surface of pyrite, the

cathodic sites were physically protected from oxidants similar to that observed in the cathodic sweep of the CV measurements.

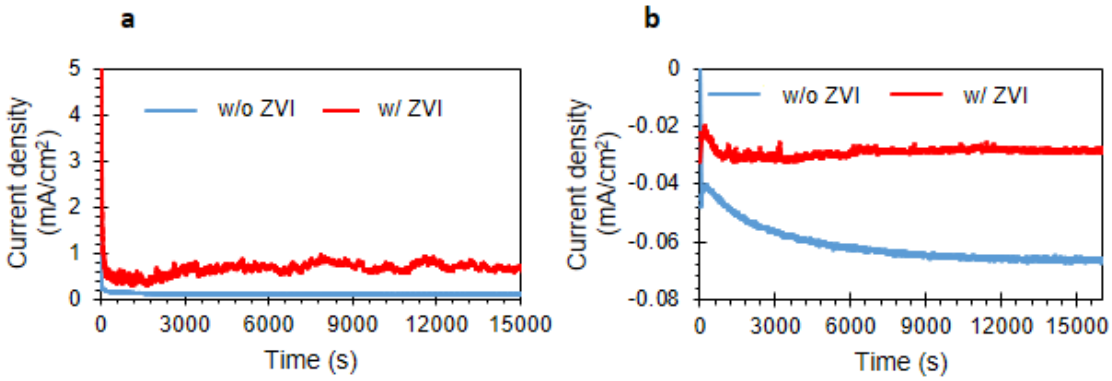

Fig. 2.10 Chronoamperometry measurements of pyrite with and without ZVI: (a) anodic polarization curves with time of pyrite with and without attached ZVI, and (b) cathodic polarization curves with time of pyrite with and without attached ZVI.

2.4 Conclusions

In this chapter, galvanic interactions of pyrite with ZVAl or ZVI under various conditions were elucidated using leaching experiments, geochemical modeling calculations, electrochemical methods, and surface characterization techniques. The results of this study are summarized as follows:

1. Both ZVAl and ZVI suppressed the oxidation of pyrite and this effect became more pronounced as the amounts of ZVAl and ZVI increased.

2. Suppressive effects of ZVAl on pyrite oxidation did not occur quickly similar to that of ZVI because of the presence of an Al-oxyhydroxide film on ZVAl. After 7 days, however, substantial suppression of pyrite oxidation was observed.

3. ZVI suppressed pyrite oxidation relatively quickly and its suppressive effects were better under acidic conditions.

4. Cyclic voltammetry and chronoamperometry confirmed that the suppressive effect of ZVAl and ZVI on pyrite oxidation was primarily due to galvanic interactions.

This chapter is edit from “Galvanic microencapsulation (GME) using zero-valent aluminum and

zero-valent iron to suppress pyrite oxidation". Materials Transactions, https://doi.org/10.2320/matertrans.M-M2018851 (Accepted) (2018)

REFERENCES

Ahlberg, E. (1990). The surface oxidation of pyrite in alkaline solution. J. Appl. Electrochem. 20 (1033-1039).

Ata, A., A. and Koldas, S., (2006). Acid mine drainage (AMD): causes, treatment and case studies, J. Clean Prod. 14 (1139-1145).

Barrie, J.D., Hallberg, K.B., (2005). Acid Mine Drainage Remediation Options: a review, J. Sci. Total Environ. 338 (3-14).

Brett, C.M., Brett, A.M.O. (1993). Electrochemistry principles, methods, and application. Oxford university press Inc., New York.

Cornell, M.R., Schwertmann, U. (2003). The Iron Oxides: Structure, properties, reaction, occurrences, and uses. 2nd edition. ISBN 3-527-30274-3

Elsetinow, A.R., Schoonen, M. A.A., Strongin, D. R. (2001). Aqueous geochemical and surface science investigation of the effect of phosphate on pyrite oxidation. 35 (2252-2257).

Evangelou, V.P. (1995). Pyrite oxidation and its control, CRC press, Boca Raton, FL.

Evangelou, V.P. (2001). Pyrite microencapsulation technology: Principles and potential field application. Ecol. Eng. 17 (165-178).

Greet, C.J., Small, G.L., Steinier, P., Grano, S.R. (2004). The magotteaux millR: investigating the effect of grinding media on pulp chemistry and flotation performance. Miner. Eng. 17:7-8 (891-896).

Heviánková, S., Bestová, I., Kyncl, M. (2014). The application of wood ash as a reagent in acid mine drainage treatment. Miner. Eng. 56 (109-111).

Huang, G. and Grano, S. (2005). Galvanic interaction of girding media with pyrite and its effect on floatation. Miner. Eng. 18 (1152-1163).

Demers, I., Benzaazoua, M., Bouda, M., Bois, D., Gagnon, M. (2015). Valorization of acid mine drainage treatment sludge as remediation component to control acid generation from mine wastes, part 1: Material characterization and laboratory kinetic testing. Miner. Eng. 76 (109-116).

Jones, A.M., Griffin, P.J., Collins, R.N., Waite, T.D. (2014). Ferrous iron oxidation under acidic condition-The effect of ferric oxide surfaces. 145 (1-12).

Kelsall, G.H., Yin, Q., Vaughan, D.J., England, K.E.R., Brandon, N.P. (1999). Electrochemical oxidation of pyrite (FeS_2) in aqueous electrolytes. J. Electroanal. Chem. 471 (116-125).

Kleinmann, R.L.P., Hedin, R.S., Nairn, R.W. (1998). Treatment of mine drainage by anoxic limestone drains and constructed wetlands. J. Environ. Sci. Springer, Berlin, Heidelberg. (303-319).

Lowson, R.T. (1982). Aqueous oxidation of pyrite by molecular oxygen. Chem. Rev. 82 (461-497).

Martin, C.J., Mclvor, R.E., Finch, J.A., Rao, S.R. (1991). Review of the effect of grinding media on flotation of sulphide minerals. Miner.eng. 4 (121-132).

Mckibben, M.A. and Barnes, H.L. (1986). Oxidation of pyrite in low-temperature acidic solution: rate laws and surface textures. Geochimica et Cosmochimica Acta, 50 (1509-1520).

Moodley, I., Sheridan, C.M., Kappelmeyer, U., Akcil, A. (2017). Environmentally sustainable acid mine drainage remediation: Research developments with a focus on waste/ by-products. Miner. Eng. http://dx.doi.org/10.1016/j.mineng.2017.08.008.

Moses, C. O. (1990). Pyrite oxidation at circumneutral pH. Geochimica. et Cosmochimica Acta. 55 (471-482).

Park, I., Tabelin, C.B., Magaribuchi, K., Seno, K., Ito, M., Hiroyoshi, N. (2018a). Suppression of the release of arsenic from arsenopyrite by carrier-microencapsulation using Ti-catechol complex. J. Hazard. Mater. 344 (322-332).

Park, I., Tabelin, C.B., Seno, K., Jeon, S., Ito, M., Hiroyoshi, N. (2018b). Simultaneous suppression of acid mine drainage formation and arsenic release by Carrier-microencapsulation using aluminum-catecholate complexes. Chemosphere. 205 (414-425).

Schweigert, N., Zehnder, A.J.B., Eggen, E.I.L. (2001). Chemical properties of catechols and their molecular modes of toxic action in cells, from microorganisms to mammals. J. Environ. Microbio. 3 (81-91).

Sánchez-España, J., Yusta, I., Diez-Ericlla, M. (2011). Schwertmannite and hydrobasaluminite: A re-evaluation of their solubility and control on the iron and aluminum concentration in acidic pit lakes. Applied Geochemi. 26 (1752-1774).

Sánchez-España, J., Yusta, I., Gray, J., Burgos, W.D. (2016). Geochemistry of dissolved aluminum at low pH: Extent and significance of Al-Fe(III) coprecipitation below pH 4.0. Geochimi. Et Cosmochimi. Acta. 175 (128-149).

Satur, J., Hiriyoshi, N., Tsunekawa, M., Ito, M., Okamoto, H. (2007). Carrier-microencapsulation for preventing pyrite oxidation. International Journal of Mineral Processing. Int. J. Miner. Process. 83 (116-124).

Sheoran, A.S., Sheoran, V. (2006). Heavy metal removal mechanism of acid mine drainage in wetlands: A critical review. Miner. Eng. 19 (105-116).

Singer, P.C., Stumm, W. (1970). Acidic mine drainage: the rate-determining step. Science. 167 (1121-1123).

Stumm, W. and Lee, F.G. (1961). Oxygenation of ferrous iron. Industrial and Eng. Chemi. 53 (143-146).

Subrahmanyam, T.V., Forssberg, K.S.E. (1993). Mineral solution-interface chemistry in minerals engineering. Miner. Eng. 6 (5) (439-454).

Tabelin, C.B., Igarashi, T., Villaurte-tabelin, V., Park, I., Opiso, E.M., Ito, M., Hiroyoshi, N. (2018). Arsenic, selenium, boron, cadminium, copper, and zinc in naturally contaminated rocks: A review of their sources, modes of environment, mechanisms of release, and mitigation strategies. Sci. Total Environ. 645 (1522-1553).

Tabelin, C.B. and Igarashi, T. (2009). Mechanisms of arsenic and lead release from hydrothermally altered rock. J. Hazard. Mater. 169 (980-990).

Tabelin, C.B., Igarashi, T., Tamoto, S. (2010). Factors affecting arsenic mobility from hydrothermally altered rock in impoundment-type in situ experiments. Miner. Eng. 23 (238-248).

Tabelin, C.B., Igarashi, T., Takahashi, R. (2012a). Mobilization and speciation of arsenic from hydrothermally altered rock in laboratory column experiments under ambient conditions. Appl. Geochem. 27 (326-342).

Tabelin, C.B., Igarashi, T., Yoneda, T. (2012b). Mobilization and speciation of arsenic from hydrothermally altered rock containing calcite and pyrite under anoxic conditions. Appl. Geochem. 27 (2300-2314).

Tabelin, C.B., Igarashi, T., Tamoto, S., Takahashi, R. (2012c). The roles of pyrite and calcite in the mobilization of arsenic and lead from hydrothermally altered rocks excavated in Hokkaido, Japan. J. Geochem. Explor. 119-120 (17-31).

Tabelin, C.B., Basri, A.H.M., Igarashi, T., Yoneda, T. (2012d). Removal of arsenic, boron, and selenium from excavated rocks by consecutive washing. Water Air Soil Poll. 223 (4153-4167).

Tabelin, C.B., Igarashi, T., Yoneda, T., Tamamura, S. (2013). Utilization of natural and artificial adsorbents in the mitigation of arsenic leached from hydrothermally altered rock. Eng. Geol. 156 (58-67).

Tabelin, C.B., Hashimoto, A., Igarashi, T., Yoneda, T. (2014a). Leaching of boron, arsenic and selenium from sedimentary rocks: I. Effects of contact time, mixing speed and liquid-to-solid ratio. Sci. Total Environ. 472 (620-629).

Tabelin, C.B., Hashimoto, A., Igarashi, T., Yoneda, T. (2014b). Leaching of boron, arsenic, and selenium from sedimentary rocks: II. pH dependence, speciation, and mechanisms of release. Sci. Total Environ. 473-474 (244-253).

Tabelin, C.B., Sasaki, R., Igarashi, T., Park, I., Tamoto, S., Arima, T., Ito, M., Hiroyoshi, N. (2017a). Simultaneous leaching of arsenite, arsenate, selenite, and selenate, and their migration in tunnel-excavated sedimentary rocks: I. Column experiments under intermittent and unsaturated flow. Chemosphere. 186 (558-569).

Tabelin, C.B., Sasaki, R., Igarashi, T., Park, I., Tamoto, S., Arima, T., Ito, M., Hiroyoshi, N. (2017b). Simultaneous leaching of arsenite, arsenate, selenite, and selenate, and their migration in tunnel-excavated sedimentary rocks: II. Kinetic and reactive transport modeling. Chemosphere. 188 (444-454).

Tabelin, C.B., Veerawattananun, S., Ito, M., Hiroyoshi, N., Igarashi, T. (2017b). Pyrite oxidation in the presence of hematite and alumina: Batch leaching experiments and kinetic modeling calculations. Sci. Total Environ. 580 (687-689).

Tabelin, C.B., Veerawattananun, S., Ito, M., Hiroyoshi, N., Igarashi, T. (2017c). Pyrite oxidation in the presence of hematite and alumina: Effects on the cathodic and anodic half-cell reactions. Sci. Total Environ. 581-582 (126-135).

Tamoto, S., Tabelin, C.B., Igarashi, T., Ito, M., Hiroyoshi, N. (2015). Short and long term release mechanisms of arsenic, selenium and boron from tunnel-excavated sedimentary rock under in situ conditions. J. Contam. Hydrol. 175-176 (60-71).

Tatsuhara, T., Arima, T., Igarashi, T., Tabelin, C.B. (2012). Combined neutralization-adsorption system for the disposal of hydrothermally altered excavated rock producing acidic leachate with hazardous elements. Eng. Geol. 139-140 (76-84).

Wiersma, C.L. and Rimstidt J.D. (1984). Rate of reaction of pyrite and marcasite with ferric ion at pH 2. Geochim. Cosmochim. Acta. 48 (85-92).

Williamson, M.A. and Rimstidt, J.D. (1994). The kinetics and electrochemical rate-determining step of aqueous pyrite oxidation. Geochim. Cosmochim. Acta 58 (5443-5454).

Wehrli, B. and Stumm W. (1989). Vanadyl in natural water adsorption and hydrolysis promote oxygenation. Geochim. Cosmochim. Acta. 53 (69-77).

Yufan, M., Yongjun, P., Rolf, A. L. (2018). The galvanic interaction between chalcopyrite and pyrite in the presence of lignosulfonate-base biopolymers and its effects on flotation performance. Miner. Eng. 122 (91-98).

Yuting, O., Yun, L., Runliang, Z., Fei, G., Tianyuan, X., Zan, L., Libo, L. (2015). Pyrite oxidation inhibition by organosilane coating for acid mine drainage control. Miner. Eng. 72 (57-64).

CHAPTER 3: PHOSPHATE-ASSISTED GALVANIC MICROENCAPSULATION USING ZERO-VALENT IRON

3.1 Introduction

In Chapter 2, GME was proposed by using ZVAl and ZVI as anodes. Eventhough pyrite oxidation was suppressed primarily due to galvanic interactions, the suppressive effects disappeared when ZVI and ZVAl were all consumed. In order to prolong the suppressive effects of GME, coating formation should be enhanced. In this chapter, phosphate is introduced to GME to enhance not only the suppression of pyrite oxidation but also coating formation. ZVAl is typically coated with Al_2O_3 that has to be removed for galvanic interaction to occur. Because of this, only ZVI was used in this chapter. Moreover, phosphate was selected to enhance coating formation because it is known to form iron phosphate, a stable material even under acidic conditions. Thus, GME using ZVI and phosphate was investigated.

3.2 Materials and methods

3.2.1 Samples

The pyrite sample used in this study was obtained from Huanzala Mine, Huanuco, Peru. The X-ray diffraction (XRD) pattern shows that it is mainly composed of pyrite and contains Fe (40.0%) and S (59.3%) as the main components with only trace impurities like silicon (0.4%), calcium (0.13%), and aluminum (0.15%) (Figs. 3.1a & b). Pyrite was crushed by a jaw crusher, ground with a ball mill, and sieved to obtain a size fraction of 500-710 μm. Ultra-pure ZVI (99.9%) used in this study was obtained from Wako Pure Chemical Industries Ltd., Japan. The particle size distribution of ZVI was measured by LASER diffraction (Microtrac® MT3300SX, Nikkiso Co. Ltd., Japan) and D_{50} was around 25 μm.

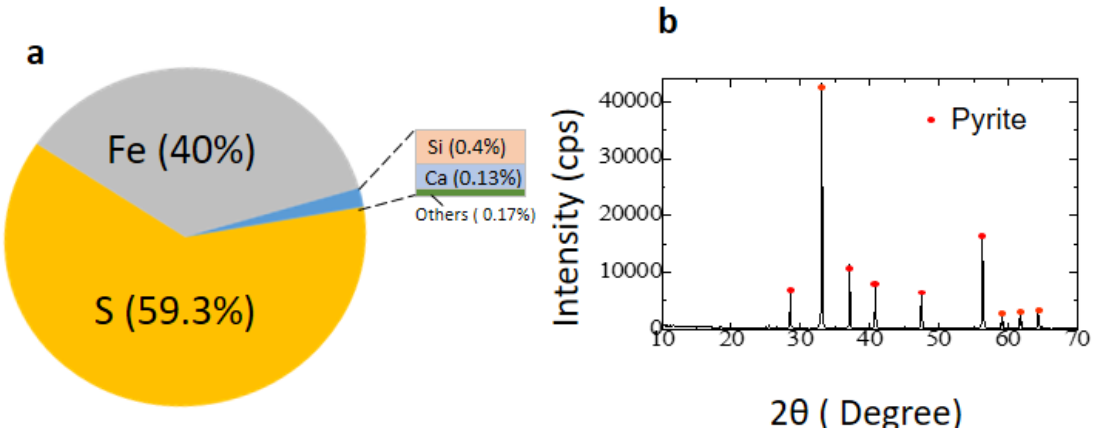

(a)

Fig. 3. 1 (a) The chemical composition and, (b) XRD pattern of pyrite sample.

3.2.2 Leaching experiments and chemical analyses

Before the leaching experiments, the pyrite sample (500-700 μm) was washed using the method described by McKibben and Barnes (1986) to remove any oxidized layer formed during sample preparation and storage. Leaching experiments were conducted by mixing 1 g of washed pyrite and 10 mL of the following solutions/suspensions: (i) deionized (DI) water (control), (ii) phosphate solution (0.2M), (iii) ZVI suspension in DI water (0.1 g/10 mL) and (iv) ZVI suspension in phosphate solution (0.1 g/ 10 mL). All solutions/suspensions were adjusted to pH 4 by adding HCl. The flasks were shaken (shaking amplitude and rate of 40 mm and 120 strokes/min, respectively) in a constant temperature water bath shaker (25 ºC).

After the predetermined leaching time, the flasks were removed from the shaker, the pH and redox potential (Eh) of suspensions were measured, and the leachates were collected by filtration through 0.2 μm syringe-driven membrane filters (Sartorius AG, Germany). The concentrations of total S as SO_4^{2-} (dissolved S), dissolved Fe, and PO_4^{3-} (dissolved P) in the filtrates were analyzed by inductively coupled plasma atomic emission spectroscopy (ICP-AES, ICPE-9820, Shimadzu Corporation, Japan) (margin of error ± 2%). Meanwhile, the residues were washed thoroughly with DI water and dried in a vacuum drying oven at 40 ºC for 24 hours. The residues were analyzed using a high-magnification optical microscope (VHX-1000, Keyence Corporation, Japan), SEM-EDX (IT-200, JEOL Ltd., Japan), some of the leaching experiments were done in triplicates to ascertain that the observed trends were statistically significant.

3.2.2 Coating experiments

Coating experiments were conducted using washed pyrite samples (500-700 μm) 1 g, 50 mM of ferrous, and 0.2 M of phosphate solution in pH 1.5, 3, and 4. These coating experiments were conducted for 1 day. The flasks were shaken (shaking amplitude and rate of 40 mm and 120 strokes/min, respectively) in a constant temperature water bath shaker (25 ºC). After the experiment, the residues were analyzed using a high-magnification optical microscope (VHX-1000, Keyence Corporation, Japan), SEM-EDX (IT-200, JEOL Ltd., Japan) and X-ray Photoelectron Spectroscopy (XPS).

Another coating experiments using synthesized $FePO_4$ with 1 g washed pyrite for 1 day. The synthesize was conducted using 50 mM Fe^{2+} and 0.2 M PO_4^{3-} in 10 mL of solution (initial pH 1.5, 3, 4, 5, and 7) and flask was shaken for 2 days at different pH under an atmospheric condition at 25 ºC to oxidize all Fe^{2+} in the solution. A 1 g of washed pyrite was added to this solution for coating experiments.

3.3 Results and discussion

3.3.1 Effects of ZVI and phosphate on pyrite oxidation

In the leaching experiments and electrochemical measurements of chapter 2, pyrite oxidation was suppressed via galvanic interaction. Although this effect was relatively rapid, it was only temporary because coating was not formed. To induce coating formation and prolong the suppression of pyrite oxidation, a combination of ZVI and phosphate (initial pH 4) was evaluated. Fig. 3.2 shows the pH, dissolved S, and Fe concentration after leaching until 7 days with/without ZVI and phosphate. The initial pH of the control (pyrite and DI water only) was around 4 but decreased to pH 3.3 after 7 days due to pyrite oxidation. When ZVI was added, the pH increased due to the reaction of ZVI with water producing OH^-. There was no significant change in pH in the presence of phosphate due to the buffering effect.

The concentration of P was almost constant with time in the absence of ZVI (Fig. 3.2b). However, the concentration of P dramatically decreased after 1 day in the presence of ZVI most probably due to precipitation of iron phosphate (Fig. 3.2b).

The precipitation of iron phosphate was also consistent with the low dissolved Fe after 1 day even at pH 4 as shown in Fig. 3.2c. When phosphate was added, the concentration of dissolved S decreased compared with the control (pyrite and DI only) (Fig. 3.2d). Suppression was even stronger when both ZVI and phosphate were present (Fig. 3.2d). Fig. 3.3 shows the SEM-EDX

results of the leaching residues after 7 days with ZVI and phosphate. A coating composed of Fe, P and O was observed on the surface of pyrite. These results indicate that iron phosphate precipitated at pH 4, coated the surface of pyrite and suppressed pyrite oxidation.

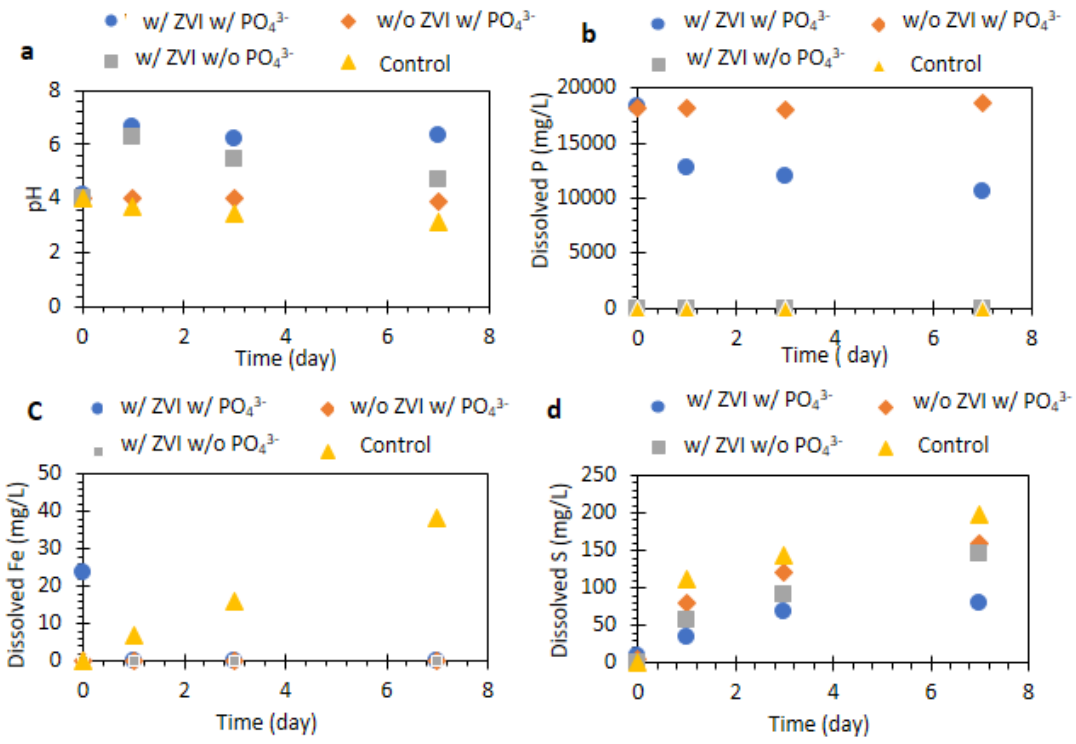

Fig. 3.2 Changes of (a) pH, (b) dissolved P, (c) dissolved Fe, and (d) dissolved S.

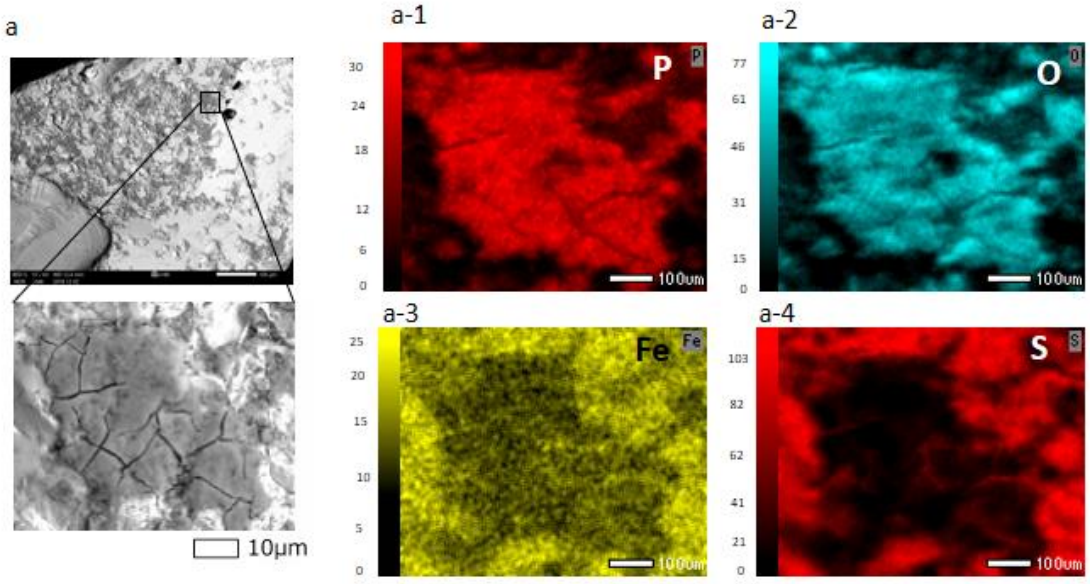

Fig. 3.3 SEM-EDX photomicrograph of pyrite after leaching for 7 days with phosphate solution and the corresponding elemental maps of (a-1) P, (a-2) O, (a-3) Fe, and (a-4) S.

3.3.2 Mechanisms of iron phosphate coating formation

There are two possible mechanisms of iron phosphate coating formation (Fig. 3.4): (1) formation of iron phosphate in bulk solution and its adsorption on the pyrite surface (Model A: bulk precipitation), and (2) Fe^{2+} oxidation on pyrite surface and the surface precipitation of iron phosphate (Model B: Surface precipitation). Although both Model A and B are pH dependent, coating formation in Model A is more extensive at higher pH while coating formation in Model B is more substantial at lower pH and will be discussed in detail below.

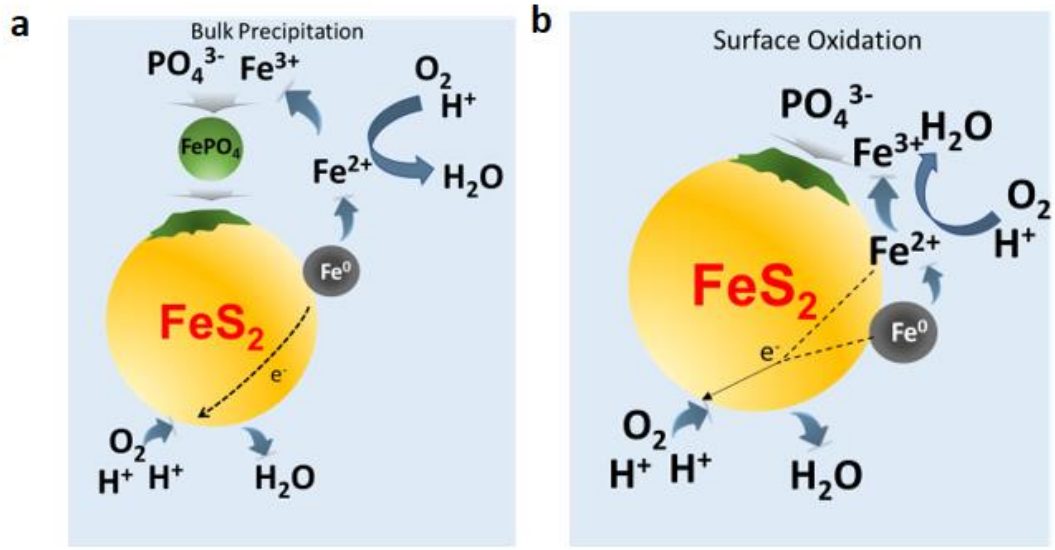

Fig. 3.4 Schematic diagram of (a) bulk precipitation model, and (b) surface precipitation model.

pH dependence of Model A and B

As described in the last section, iron phosphate precipitate formed in bulk solution phase is the substance to form coating in Model A but Fe^{2+} in the solution is the substance in Model B. It has been reported that Fe^{2+} oxidation rate in bulk solution depend on pH: oxidation rate of Fe^{2+} increases with increasing pH (Stumm and Lee, 1961). Because of this, Fe^{2+} concentration remained in the solution phase decrease with increasing pH and the amount of iron phosphate precipitate increases with pH. This pH dependence of Fe^{2+} concentration and iron phosphate precipitation would cause the coating formed on the pyrite surface.

In the case of Model A, iron phosphate precipitated in the bulk solution phase adsorbs on the pyrite surface to form the coating. If the attraction between pyrite and iron phosphate is assumed to be independent of pH, the coating formed by the adsorption of precipitate on pyrite surface would become thicker with increasing pH, since larger amount of precipitate is formed at higher pH.

In the case of Model B, Fe^{2+} is oxidized on the surface of pyrite to form the coating. When pyrite amount is small and the surface area is limited in the system, oxidation of Fe^{2+} on the pyrite surface can be assumed to be slower than in bulk solution phase. If this is the case, the coating formed by the surface precipitate on pyrite would become thicker with decreasing pH, since a larger amount of Fe^{2+} has remained in the solution at lower pH.

As discussed above, pH dependence of coating formation is different in Models A and B. To confirm the pH dependence, coating experiments were carried out. A 1 g of pyrite was shaken in 10 mL of a solution containing 50 mM Fe^{2+} and 0.2 M PO_4^{3-} at different initial pH for 1 day under an atmospheric condition at 25 ^oC.

Fig. 3.5 shows the results of SEM-EDX analysis for the solid residue treated at different pH. At lower pH, strong P and O signals were detected. Meanwhile, S signal becomes weaker at lower pH. These results are in line with the assumption that thicker coating is formed at lower pH. SEM images (Fig. 3.5a) showed that the surface structure was smooth and homogenous at pH 4 but the surface became cracked and rough at lower pH. These cracks may be formed by the breaking of thicker layer formed at lower pH because of drying during the sample preparation. These results suggest that model B (surface precipitation model) is probably more dominant than model A (bulk precipitation).

Coating experiments of pyrite with synthesized ferric phosphate powder (< 5μm) in DI water for 1 day was carried out. Fig. 3.6 shows SEM-EDX of the leaching residue showed that negligible amounts of a coating were formed and this indicates that coating formation by model A may not occur.

These results support that model B (surface precipitation model) is the main mechanism for the coating formation. In the model B, the coating is formed in the presence of Fe^{2+}, PO_4^{3-}, and O_2. To elucidate these materials on the coating formation, coating experiments were carried out with and without these materials at initial pH of 1.5. The results of SEM-EDX analysis of the treated pyrite indicated that there is no coating when either Fe^{2+}, PO_4^{3-}, or O_2 is absent. This confirms that these three material are essentials to form a coating as predicted from model B.

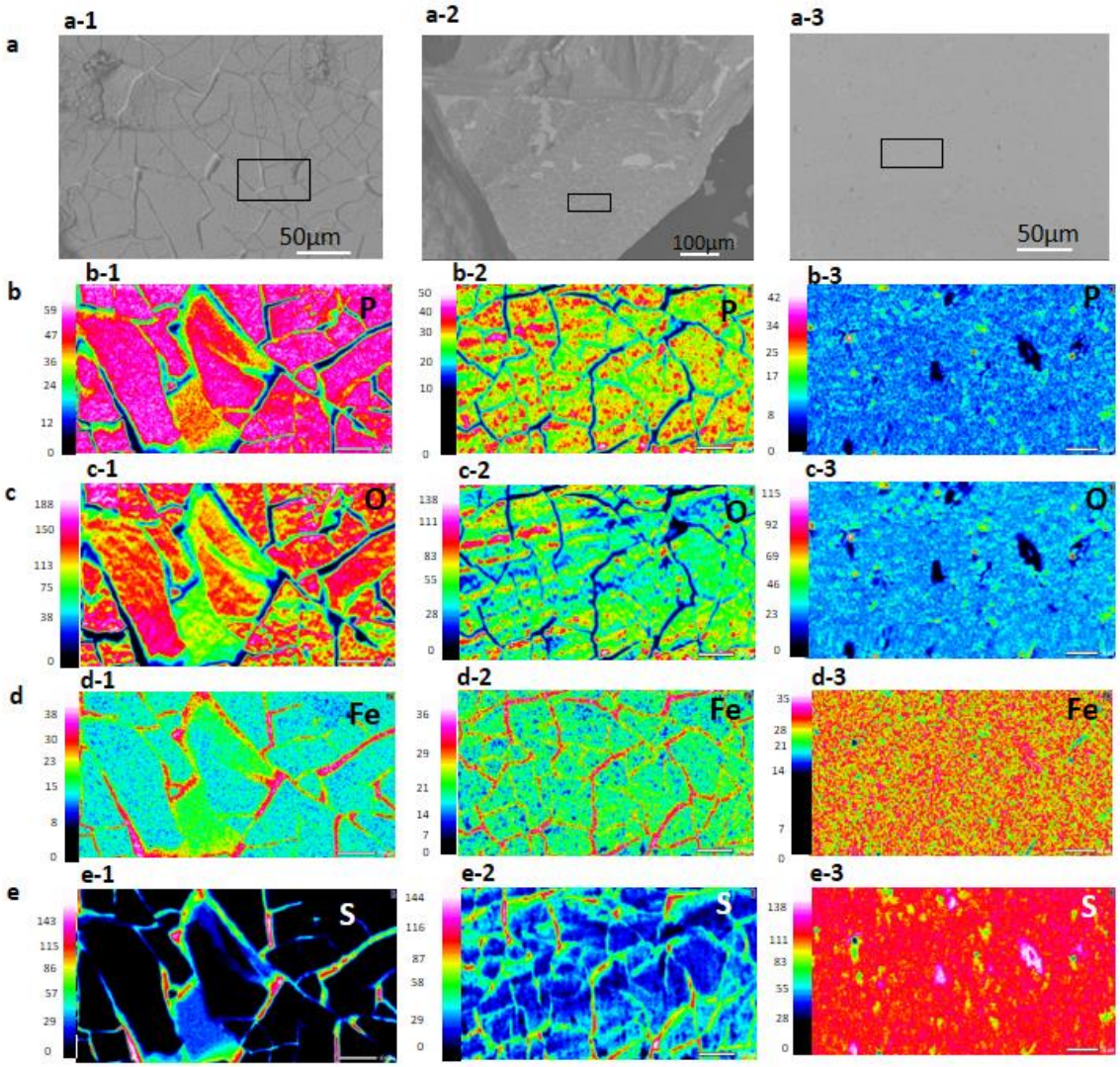

Fig. 3.5 SEM-EDX photomicrograph of pyrite residue in pH (a-1) 1.5 , (a-2) 3, and (a-3) 4, (b) elemental mapping of P in (b-1) pH 1.5, (b-2) pH 3, and (b-3) pH 4, (c) elemental mapping of O in (c-1) pH 1.5, (c-2) pH 3, and (c-3) pH 4, (d) elemental mapping of Fe in (d-1) pH 1.5, (d-2) pH 3, and (d-3) pH 4, and (e) elemental mapping of S in (e-1) pH 1.5, (e-2) pH 3, and (e-3) pH 4.

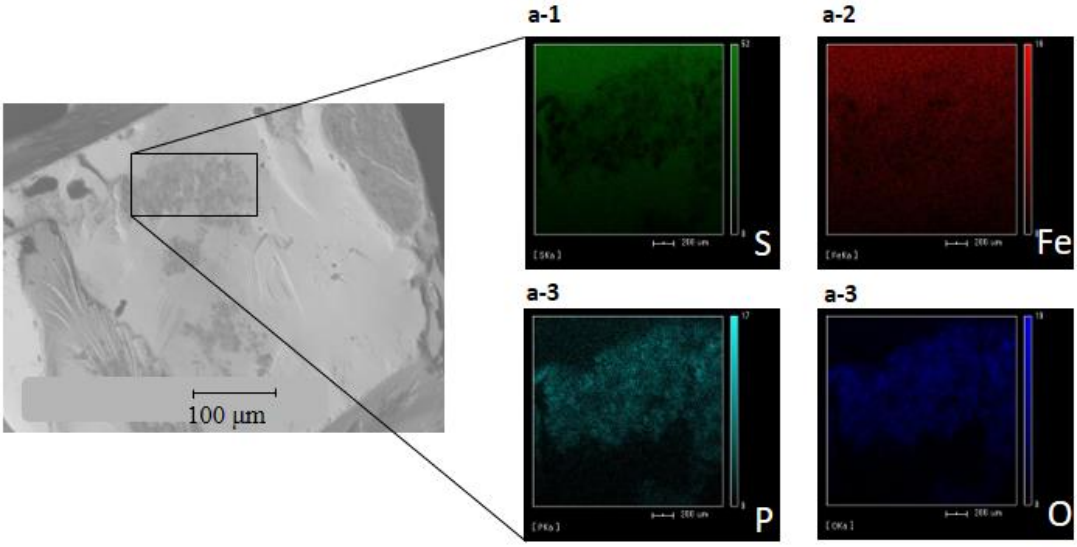

Fig. 3.6 SEM-EDX photomicrograph of pyrite residue.

3.4 Conclusions

The iron phosphate coating formed on the pyrite surface may occur via the following two mechanisms: (1) formation of iron phosphate in solution and its adsorption on the pyrite surface (model A), (2) the formation of iron phosphate coating directly on the pyrite surface (model B).

REFERENCE

Nyavor, K., Egiebor, N.O. (1995). Control of pyrite oxidation by phosphate coating. Sic. Total Env. 162 (225-237).

Stumm, W., Lee, G.F. (1961). Oxygenation of ferrous iron. Industrial and Eng. Chemi. 53 (143-146)

CHAPTER 4: GALVANIC MICROENCAPSULATION USING PHOSPHATE AND BALL MILL

4.1 Introduction

In chapter 3, the mechanism of ferric phosphate coating formation was discussed and the results suggest that coating formation by model B may occur under acidic conditions at around pH 4. In this chapter, the possible application of GME using phosphate and ball mill with steel ball media as iron sources was investigated. Fig. 4.1 shows a schematic diagram of how GME happens inside the ball mill using steel ball media in the presence of phosphate. In mineral processing, pyrite is the most common gangue mineral of non-ferrous sulfide ores, which means that tailings contain pyrite that is the main cause of acid mine drainage (AMD). If pyrite can be coated during the mineral processing of the ore, then AMD formation in the tailings dam will be greatly limited. Moreover, the formation of iron phosphate, a hydrophilic phase, can be beneficial during flotation (e.g., coal).

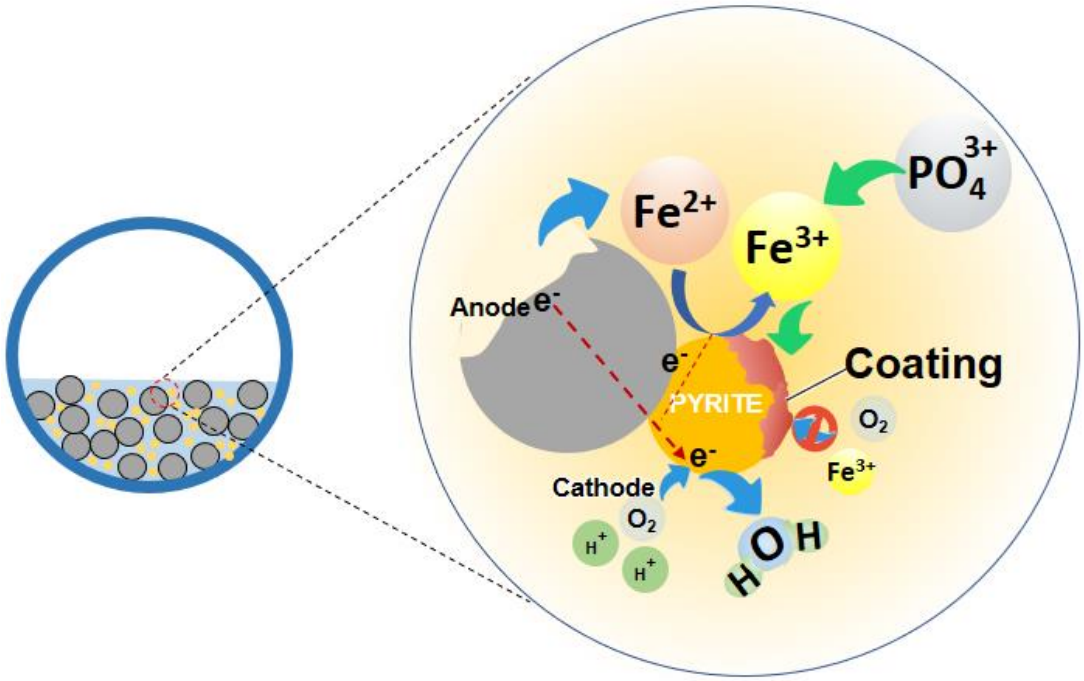

Fig. 4.1 A schematic diagram of galvanic interaction between steel balls and pyrite inside the ball mill.

4.2 Materials and methods

4.2.1 Materials

The pyrite sample used in this study was obtained from Huanzala Mine, Huanuco, Peru. The X-ray diffraction (XRD) pattern showed that it is mainly composed of pyrite and contains Fe (44%) and S (59.3%) as the main components with only trace impurities like silicon (0.4%), calcium (0.13%), and aluminum (0.15%) (Chapter 3). Pyrite was crushed by a jaw crusher, ground with a ball mill, and sieved to obtain a size fraction of 500-710 μm.

4.2.2 Ball mill and leaching experiments

Wet grinding was conducted by using 100 g of pyrite samples (size 500-700 μm) with steel balls (diameter 0.6 cm) with and without phosphate (50mM), and the combination of phosphate and intermittent air induction in a mill pot with a diameter of 8 cm. This grinding continues for 3 hours. After ball milling, the balls were removed by hand and pyrite was washed six times with DI water.

Leaching experiments were conducted by mixing 1 g of pyrite (obtained after ball milling), 10 mL of deionized (DI) water for 7 days. The flasks were shaken (shaking amplitude and rate of 40 mm and 120 strokes/min, respectively) in a constant temperature water bath shaker (25 ºC). After the predetermined leaching time, the flasks were removed from the shaker, the pH and redox potential (Eh) of suspensions were measured, and the leachates were collected by filtration through 0.2 μm syringe-driven membrane filters (Sartorius AG, Germany). The concentrations of total S as SO_4^{2-} (dissolved S), dissolved Fe were analyzed by inductively coupled plasma atomic emission spectroscopy (ICP-AES, ICPE-9820, Shimadzu Corporation, Japan) (margin of error ± 2%). Meanwhile, the residues were washed thoroughly with DI water and dried in a vacuum drying oven at 40 ºC for 24 h. The residues were analyzed using a high-magnification optical microscope (VHX-1000, Keyence Corporation, Japan), SEM-EDX (SSX-550, Shimadzu Corporation, Japan), some of the leaching experiments were done in triplicates to ascertain that the observed trends were statistically significant.

4.2.3 Flotation experiments

Coal flotation experiments were carried out using mixture of 16 g of Kushiro coal (100-150 μm), 3g of pyrite (with and without coating, 100-150 μm), and 1 g of quartz (100-150 μm). The modified tree analysis method of Tsunekawa et al. (Tsunekawa, M. et al., 1998) was used.

Flotation tests were carried out in an Agitair-type batch flotation cell (FT-1000, Heiko, Japan) with 400 mL suspension containing 20 g of samples. The impeller speed was 1000 rpm and the aeration rate was 0.75 L/min. The suspension was agitated for 3 min and then 15 μL of MIBC was added and agitated for 3 min and air was introduced for flotation. Froth products were recovered for 3 min wihout a collector, then 15 μL of MIBC was added and agitated for 3 min and 2 μL of kerosene (collector) was added and agitated for 3 min, air was introduced and froth products were recovered for 3 min. This procedure was repeated with 3, 5, 5 μL of additional kerosene (cumulative kerosene volume were 2, 5, 10, and 15μL). The froth products were collected separrately from each flotation stage and ash value of the froth and taillings products were determined according to the Japanese Industrial Standards (JIS) (M8812).

4.3 Results and discussion

4.3.1 Ball mill treatment

Preliminary ball mill experiments with steel ball media were carried out with and without phosphate. The results showed that dissolved Fe concentrations remained high (110 mg/L) even though the pH was around 5, which suggests that the supply of oxygen was not enough to oxidize ferrous to ferric. Because of this, another experiment was conducted with intermittent air induction. The results showed that dissolved Fe concentrations after ball milling with air induction decreased by less than 10 mg/L because of oxidation of ferrous by oxygen suggesting that enough oxygen was presented.

4.3.2 Leaching of ball mill products

Ball mill products were leached in DI water until 7 days to evaluate the suppression of pyrite oxidation by iron phosphate coating formation during ball mill. The leaching results showed that the S and Fe concentrations were lower with phosphate and air induction (Fig. 4.2). SEM-EDX observation of leaching residue (Fig. 4.3) showed that in some areas strong signals of O and P, weak signals of S and Fe were detected. This indicates that the surface of pyrite was coated with a Fe-P-O containing phase. This means that phosphate addition during ball milling using steel ball media can passivate pyrite by forming iron phosphate coating.

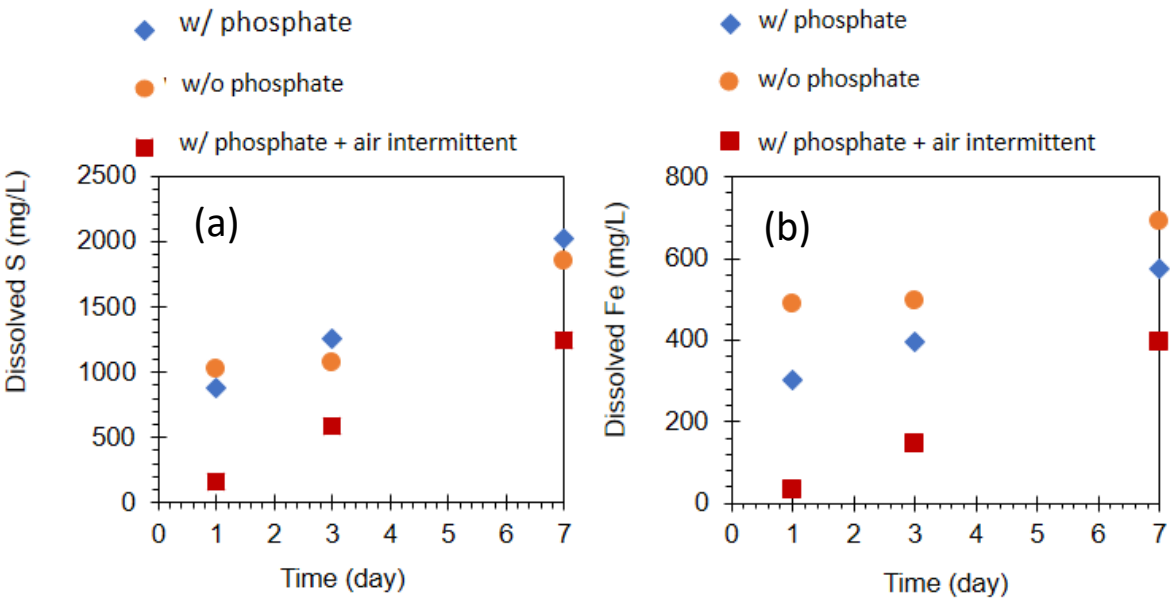

Fig. 4. 2 Change of (a) dissolved S, and (b) final Fe.

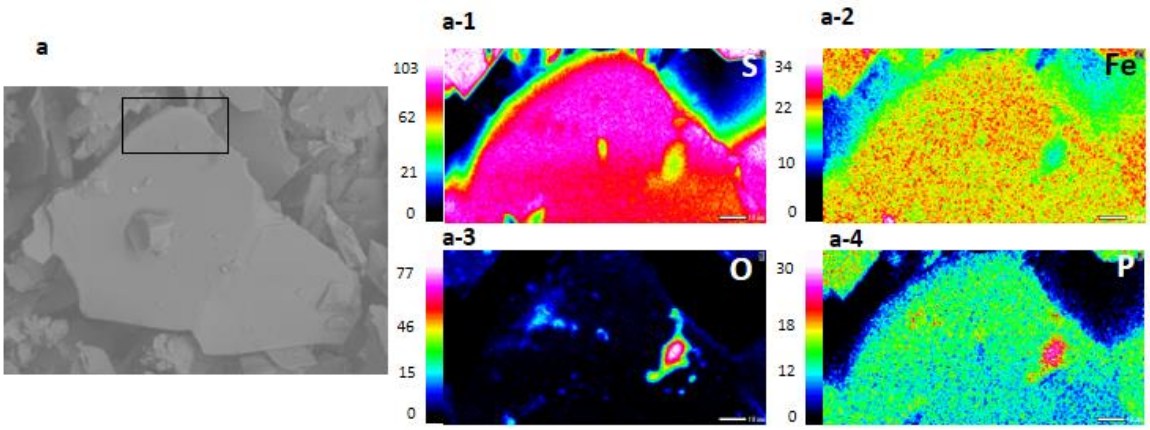

Fig. 4. 3 SEM-EDX photomicrograph of pyrite after leaching for 1 day with DI water and the corresponding elemental maps of (a-1) S, (a-2) Fe, (a-3) O, and (a-4) P.

4.3.3 Flotation experiments

The results of coal flotation (combustible or ash recovery versus yield) are plotted in Fig. 4.4. The Kushiro coal sample, which contains organic matter and gangue minerals, was mixed with pyrite and quartz for the flotation experiments, so after ashing, the ash contains both mineral matter from

the coal and those from pyrite and quartz added to the coal sample. Higher ash recovery and smaller hatched line area indicate that gangue minerals containing pyrite are entrained in froth products. The results showed that the area of hatched line of (a) without GME was smaller than that of (b) with GME, suggesting that entrainment of pyrite to the froth became smaller due to the hydrophilic coating on pyrite after GME. These results suggest that pyrite coating by GME using a ball mill is possible, which could not only improve the separation efficiency of coal and pyrite but also suppress AMD generation by forming protective coatings on pyrite.

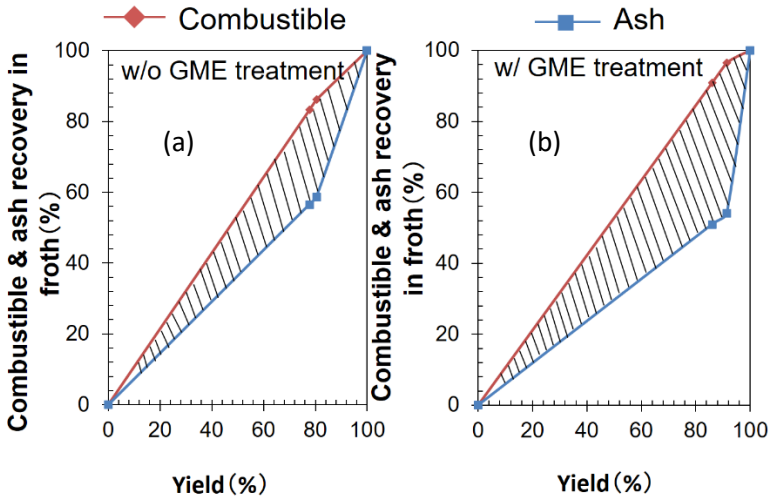

Fig. 4. 4 Combustible and ash recovery of coal (a) without and (b) with GME treatment.

4.4 Conclusions

In this chapter, the possible application of GME using phosphate and ball mill with steel ball media was investigated and phosphate addition during ball milling using steel ball media can passivate pyrite by forming iron phosphate coating. This coating treatment could improve separation efficiency of valuable minerals (e.g., coal) as froth and pyrite as tailings.

REFERENCES

Fuerstenau D.W., P.H. Metzger, G.D. Seele. (1957). How to use this modified Hallimond tube for better flotation testing, Engineering and Mining Journal, 158 (93–95).

Wills B.A., Mineral Processing Technology. (1997) An Introduction to the Practical Aspects of Ore Treatment and Mineral Recovery", 6th ed. Butterworth Heinemann, Massachusetts.

Wills B. A., Mineral processing technology. (2006) An introduction to the practical aspects of ore treatment and mineral recovery, seventh ed., Elsevier, Butterworth Heinemann, London (289).

CHAPTER 5: GENERAL CONCLUSIONS

Acid mine drainage (AMD) is one of the biggest environmental concerns for centuries. This problem is generally caused by the exposure of sulfide minerals to oxygen and water, which can occur naturally. However, mining and mineral processing industries exacerbate the problem because they generate and expose large volume of pyrite-rich wastes to the environment. AMD is very acidic (pH<3) and contains high concentrations of hazardous heavy metals such as copper (Cu), lead (Pb), and zinc (Zn) as well as toxic metalloids like arsenic (As) and selenium (Se). The most widely used technique to mitigate the negative environmental impacts of AMD is via neutralization. In this technique, basic materials such as limestone are added to AMD to increase its pH and precipitate most of the heavy metals as metal oxyhydroxides. Even though this technique is effective, AMD generation could continue for several decades or even centuries, so this approach is unsustainable. Microencapsulation is a promising and potentially more sustainable approach because it limits AMD production by suppressing pyrite oxidation directly through the formation of a passivating coating on the mineral, so this study developed a new microencapsulation technique to prevent pyrite oxidation called Galvanic microencapsulation (GME).

Chapter 1 gives a general introduction of acid mine drainage (AMD) formation, traditional neutralization techniques, and previously developed microencapsulation techniques. The statement of the problem and objectives of the study are highlighted to understand the key points and the structure of the entire research. Remediation and prevention techniques were also reviewed. AMD is typically treated by passive and active techniques. The current passive techniques used for AMD are anoxic limestone drains (ALD), aerobic wetlands, anaerobic wetlands/ compost bioreactors, permeable reactive barriers and packed bed iron-oxidation bioreactors. Active processes use basic materials such as limestone to raise the pH of AMD followed by sedimentation of the precipitated sludge. Because pyrite is the primary source of AMD, the concept of microencapsulation to form a protective coating on the pyrite surface to prevent oxidation and AMD generation is recently gaining attention. The original microencapsulation techniques introduced by Evangelou (2001) used hydrogen peroxide (H_2O_2) to oxidize Fe^{2+} to Fe^{3+} for the formation of insoluble ferric phosphate on pyrite. Although this technique effectively suppressed pyrite oxidation, H_2O_2 was unable to selectively target pyrite in real, complex wastes leading to unnecessarily large consumption of expensive reagents. Moreover, handling and storage of H_2O_2 are both difficult, especially in large-scale applications. Carrier

microencapsulation (CME) is, a microencapsulation technique that uses redox-sensitive metal(loid)-organic complexes to carry the coating material to the surface of pyrite where the complexes are adsorbed and decomposed, releasing the insoluble metal(loid) ion of the complex that is rapidly precipitated to form a protective coating on pyrite. Because pyrite dissolves via an electrochemical mechanism, the redox-sensitive metal (loid)-organic complexes have been shown to selectively target pyrite even in a complex system containing arsenopyrite and quartz. One current limitation of this technique is the use of catechol, which when oxidated in the presence of DO and metal ions like Fe^{3+} and Cu^{2+} forms semiquinone radicals, superoxides, and H_2O_2 that are toxic to cells.

Chapter 2 introduces a new encapsulation technique, called galvanic microencapsulation (GME). The effects of GME on pyrite oxidation using zero-valent aluminum (ZVAl) or zero-valent iron (ZVI) at various dosages and under different conditions (leaching time and pH) were investigated. Pyrite oxidation was suppressed in the presence of ZVAl or ZVI. Pyrite oxidation suppression mechanisms by GME during leaching were elucidated by electrochemical measurements. Cyclic voltammetry and chronoamperometry measurements showed that the suppressive effects of ZVAl and ZVI were predominantly due to galvanic interactions.

In chapter 3, a coating technique for the prolonged suppression of pyrite oxidation using phosphate and ZVI was developed. In chapter 2 galvanic interaction was observed, however, there was no coating formation on the pyrite surface. In the presence of phosphate, suppression of pyrite oxidation by ZVI was dramatically improved because of the combined effects of galvanic interactions and coating formation. The mechanism of protection could be explained as follows: (i) ZVI was oxidized on pyrite surface, (ii) ferrous ions are released, and (iii) ferrous ions are oxidized to ferric ion in the presence of oxygen. When phosphate and ZVI were added, ferric phosphate was formed as a protective coating on pyrite surface. There are two possible mechanisms: (1) formation of iron phosphate in solution and its adsorption on the pyrite surface (Model A) and (2) the formation of iron phosphate coating directly on the pyrite surface (Model B). Experimental results showed that with the addition of synthesized iron phosphate, no coating was detected, indicating that Model A is not the main mechanism of coating formation. Coating experiments using Fe^{2+} and phosphate ion at different pH showed that a thicker coating was formed on the pyrite surface at lower pH, suggesting that Model B is the main mechanism of coating formation.

In Chapter 4, possible application of GME using phosphate and ball mill with steel ball media was investigated. In mineral processing, pyrite is the most common gangue mineral of non-ferrous sulfide ores, which means that tailings contain pyrite that is the main cause of acid mine drainage

(AMD). If pyrite can be coated during mineral processing of the ore then AMD formation in the tailings dam will be greatly limited. Moreover, the formation of iron phosphate, which is hydrophilic, can be beneficial during flotation (e.g., coal). GME treatment during ball milling in the presence of phosphate was carried out and leachability of ball mill product was evaluated. The results showed that the addition of phosphate during ball milling using a steel ball media can passivate pyrite by forming iron phosphate coating. Coal flotation experiments using mixture of coal, quartz, and pyrite were carried out with and without GME treatments. The results showed that GME treatment improved the separation efficiency of coal and gangue minerals including pyrite.